

Old Dominion University ODU Digital Commons

CCPO Publications

Center for Coastal Physical Oceanography

2004

Satellite Evidence of Hurricane-Induced Phytoplankton Blooms in an Oceanic Desert


S. M. Babin

J. A. Carton

T. D. Dickey

J. D. Wiggert
Old Dominion University

Follow this and additional works at: https://digitalcommons.odu.edu/ccpo_pubs

 Part of the [Atmospheric Sciences Commons](#), [Oceanography Commons](#), and the [Remote Sensing Commons](#)

Repository Citation

Babin, S. M.; Carton, J. A.; Dickey, T. D.; and Wiggert, J. D., "Satellite Evidence of Hurricane-Induced Phytoplankton Blooms in an Oceanic Desert" (2004). *CCPO Publications*. 264.
https://digitalcommons.odu.edu/ccpo_pubs/264

Original Publication Citation

Babin, S. M., Carton, J. A., Dickey, T. D., & Wiggert, J. D. (2004). Satellite evidence of hurricane-induced phytoplankton blooms in an oceanic desert. *Journal of Geophysical Research: Oceans*, 109(C3), C03043. doi:10.1029/2003jc001938

This Article is brought to you for free and open access by the Center for Coastal Physical Oceanography at ODU Digital Commons. It has been accepted for inclusion in CCPO Publications by an authorized administrator of ODU Digital Commons. For more information, please contact digitalcommons@odu.edu.

Satellite evidence of hurricane-induced phytoplankton blooms in an oceanic desert

S. M. Babin,¹ J. A. Carton,² T. D. Dickey,³ and J. D. Wiggert⁴

Received 29 April 2003; revised 8 December 2003; accepted 21 January 2004; published 25 March 2004.

[1] The physical effects of hurricanes include deepening of the mixed layer and decreasing of the sea surface temperature in response to entrainment, curl-induced upwelling, and increased upper ocean cooling. However, the biological effects of hurricanes remain relatively unexplored. In this paper, we examine the passages of 13 hurricanes through the Sargasso Sea region of the North Atlantic during the years 1998 through 2001. Remotely sensed ocean color shows increased concentrations of surface chlorophyll within the cool wakes of the hurricanes, apparently in response to the injection of nutrients and/or biogenic pigments into the oligotrophic surface waters. This increase in post-storm surface chlorophyll concentration usually lasted 2–3 weeks before it returned to its nominal pre-hurricane level. *INDEX TERMS*: 0315 Atmospheric Composition and Structure: Biosphere/atmosphere interactions; 1640 Global Change: Remote sensing; 4504 Oceanography: Physical: Air/sea interactions (0312); *KEYWORDS*: phytoplankton, hurricane wakes, chlorophyll

Citation: Babin, S. M., J. A. Carton, T. D. Dickey, and J. D. Wiggert (2004), Satellite evidence of hurricane-induced phytoplankton blooms in an oceanic desert, *J. Geophys. Res.*, 109, C03043, doi:10.1029/2003JC001938.

1. Introduction

[2] The Sargasso Sea spans the subtropical gyre roughly between 20°N and 35°N and 70°W and 30°W, bounded by the North Equatorial Current to the south and the Gulf Stream to the north and west. In winter, climatological sea surface temperatures (SSTs) range from 19°C in the northeast to 26°C in the southwest while, in the summer, these SSTs range from 24°C in the east to 28°C in the west. The comprehensive in situ measurements made as part of the Bermuda Atlantic Time series Study (BATS) and the Bermuda Testbed Mooring (BTM) programs provide a picture of seasonal cycles of physical and biogeochemical processes in the northern Sargasso Sea. Mixed-layer depth at the BATS/BTM sites (approximately 32°N, 64°W) ranges from greater than 170 m in winter to as shallow as 10–20 m during the summer [Steinberg *et al.*, 2001; Dickey *et al.*, 1998a, 2001]. The mean permanent pycnocline depth is greater than 500 m, with a shallower isothermal layer of subtropical mode water (temperature 18°C) that is evident over much of the domain and thought to be formed during seasonal convection [Talley and Raymer, 1982]. Wintertime convection occurs in the northern Sargasso Sea as a result of wind mixing and heat loss. Such convective mixing is

much less evident in the southern Sargasso Sea, where the seasonal SST variation is only a few degrees.

[3] Nutrient availability in the euphotic zone is closely linked to the seasonal mixed-layer evolution, with wintertime nitrate concentrations typically reaching 1 μM when subtropical (18°C) mode water ventilates to the north [Steinberg *et al.*, 2001, and references therein]. In the southern Sargasso Sea, this typically does not occur so winter nutrient enrichment is less pronounced. During this nutrient enrichment period, phytoplankton growth is light-limited, as the depth of the mixed layer exceeds the critical depth so that an accumulation of phytoplankton biomass cannot occur [Siegel *et al.*, 2002]. It is also noteworthy that mesoscale eddies that have been observed near the BATS/BTM sites can result in nutrient injections into the euphotic layer, elevated primary production, and increases in organic particle fluxes to depth [e.g., McNeil *et al.*, 1999; Dickey *et al.*, 2001; Conte *et al.*, 2003].

[4] When the mixed layer shoals during March–April, the spring phytoplankton bloom is triggered, extending northward over time [Siegel *et al.*, 1990]. This spring bloom rapidly utilizes the nutrients in the surface waters, and the subsurface deep chlorophyll maximum (DCM) begins to develop, as water column stratification continues to intensify below the shallow 15–25 m mixed layer/seasonal thermocline from late spring to early fall. The seasonal thermocline inhibits further nutrient enrichment of the surface waters. The DCM manifests below the mixed layer at the depth where turbulent diffusion or breaking internal gravity waves maintain nutrient concentrations sufficient to sustain ample rates of primary productivity given the ambient light field [Varela *et al.*, 1992]. The DCM's seasonal deepening relates primarily to the seasonal increase in short wave insolation. At the BATS site, the DCM typically is concentrated between 60 and 100 m and then

¹Johns Hopkins University Applied Physics Laboratory, Laurel, Maryland, USA.

²Department of Meteorology, University of Maryland, College Park, Maryland, USA.

³Ocean Physics Laboratory, University of California, Santa Barbara, Goleta, California, USA.

⁴Center for Coastal Physical Oceanography, Old Dominion University, Norfolk, Virginia, USA.

deepens through the fall. Episodic forcing by mesoscale eddies and strong wind events plays an important role in establishing the detailed progression of the seasonal cycle just described.

[5] Hurricane-force winds (speeds greater than 33 m s^{-1}) have dramatic effects on the upper ocean. Frequently, near-surface waters cool several degrees C as mixed layers deepen by tens of meters with the most intense changes occurring under the more intense winds on the right-hand side (left-hand side in the Southern Hemisphere) of the storm track [Hazelworth, 1968; Dickey and Simpson, 1983; Stramma et al., 1986; Sanford et al., 1987]. Conversely, downward mixing of heat causes the upper seasonal thermocline waters to warm. High-amplitude near-inertial internal gravity waves (with vertical displacements of isotherms of a few tens of meters) and currents (around 1 m s^{-1}) are induced, which persist for several days, and geostrophic flows may be produced also [Shay and Elsberry, 1987; Shay et al., 1989, 1990; Dickey et al., 1998b; Zedler et al., 2002]. The SST decrease is a result of both enhanced vertical mixing and upwelling induced by a near-inertial response of the oceanic mixed layer to the asymmetric surface wind stress [Price, 1981; Shay and Elsberry, 1987], as well as flux-induced cooling.

[6] The upper ocean response to a particular hurricane depends on several parameters involving atmospheric and oceanic variables [e.g., Price, 1981; Dickey et al., 1998b]. Some of the important atmospheric variables include hurricane size (e.g., radius of tropical storm force winds, radius of hurricane-force winds), strength (wind speed), and transit speed. Local hydrodynamic conditions (i.e., pre-existing stratification and near-inertial currents) also play important roles in oceanic response to a hurricane, while the vertical distribution of nutrients and phytoplankton are primary factors in defining the resulting biogeochemical response. Implicit in these pre-hurricane conditions is the possibility that a hurricane can pass through the same area as a previous hurricane so that the post-hurricane conditions of the first storm become the pre-hurricane conditions of the subsequent storm (cases like this are discussed below).

[7] Although the biological response of the open ocean to hurricane-force winds is poorly understood at present, increases in phytoplankton concentration have commonly been observed in oceanic regions subject to coastal upwelling [e.g., Sousa and Bricaud, 1992], upwelling associated with oceanic fronts [Strass, 1992], and upwelling associated with mesoscale eddies [McGillicuddy and Robinson, 1997; McNeil et al., 1999; McGillicuddy et al., 1998, 2001]. Oceanic upwelling results in an increase in near-surface phytoplankton because phytoplankton are brought closer to the surface so that their photosynthetic system receives greater solar irradiance and because requisite nutrients are transported into the euphotic zone. Potential hurricane impacts include changes in upper ocean biogeochemistry such as enhanced efflux of carbon dioxide to the atmosphere [e.g., Bates et al., 1998], triggering of episodic export production that would tend to counter this carbon dioxide efflux, and modification of upper ocean heating rates and heat fluxes as phytoplankton blooms modulate the magnitude of downwelling irradiance [e.g., Dickey and Falkowski, 2002].

[8] The Bermuda Testbed Mooring (BTM), located 80 km southeast of Bermuda in 4.4-km-deep waters, has made the only in situ measurements of both physical and bio-optical properties in the Sargasso Sea associated with a hurricane passage (1995 Hurricane Felix and 2003 Hurricane Fabian) of which we are aware [Dickey et al., 1998a, 1998b; Zedler et al., 2002]. Unfortunately, no simultaneous satellite-based ocean color observations were available over the region to complement this in situ response data set for Hurricane Felix. The BTM data for Hurricane Fabian will be recovered in November 2003. However, our preliminary interdisciplinary modeling study suggested that an increase in chlorophyll (chl-a) associated with a phytoplankton bloom could result under suitable conditions following hurricane passage [Babin et al., 2002].

[9] The present study therefore exploits the broad spatial coverage of satellite observations of chl-a and SST to examine the biological and physical response of the mixed layer to hurricane forcing. In an effort to simplify the process of identifying pertinent mechanisms contributing to these responses, we select for this study a geographic domain consisting of a box bounded by latitudes 20°N to 32°N and longitudes 55°W to 78°W (Figure 1). This region will be defined herein as “the box” and is a region of oligotrophic open ocean unaffected by coastal or bottom influences. The waters of this region are considered to be optical Case 1 in classification [Morel and Prieur, 1977], meaning that phytoplankton and their biological products, rather than terrigenous materials, are primarily responsible for variations in optical properties. Chromophoric dissolved organic matter (also known as CDOM or gelbstoffe) makes relatively small contributions to the optical properties in Case 1 waters.

[10] We will focus our investigation on hurricanes that cross this box during the Atlantic hurricane season of June 1 to November 30. For each of these hurricanes, we estimate key physical and biological characteristics in an effort to quantify the hurricane-induced ecosystem response in an oligotrophic regime. Only the years 1998 through 2001 will be examined, and each of these years had what the National Hurricane Center (NHC) characterized as above-normal activity. Interestingly, the last 6 years of the twentieth century are among the most impressive in modern record with a 2.5-fold increase in hurricanes with sustained winds exceeding 50 m s^{-1} . This increase in hurricane activity may be related to greater SSTs and less vertical wind shear in regions where hurricanes are spawned [Elsner, 2003]. The year 1998 is chosen as a starting point because that was the first complete Atlantic hurricane season for which satellite-derived chl-a data from the Sea-viewing Wide Field-of-view Sensor (SeaWiFS) were available.

[11] For the remainder of this paper, we first present the methods used in this study, including the use of data sets containing relevant physical and biological data over the western North Atlantic Ocean during the hurricane seasons of 1998 through 2001. Next, the remote sensing chl-a and SST observations are described in the context of the NHC reports for each storm and for each year's Atlantic hurricane season. We then provide an illustrative example of how the remote sensing observations are used to determine chl-a and SST before and after a particular hurricane passage (1998 Bonnie). Our analysis of the remote sensing results and a

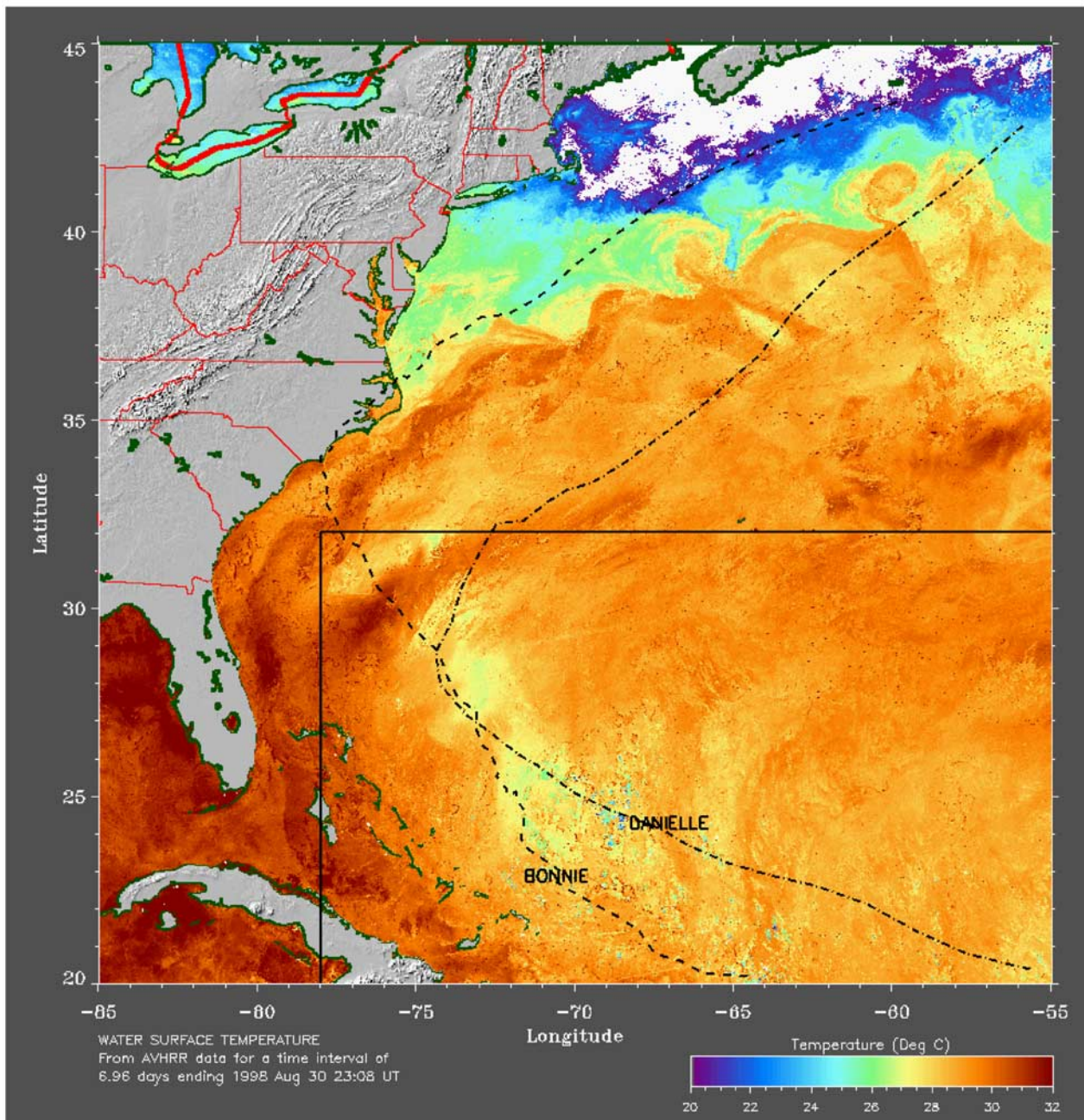


Figure 1. The 7-day composite sea surface temperature data acquired 30 August 1998 from NOAA-12 and NOAA-14. The box defined in the text is outlined. The tracks of 1998 Bonnie and Danielle are superimposed.

discussion of possible explanations for the occurrence of hurricane-induced surface chl-a enhancements are then presented.

2. Methods

2.1. Parameters Derived From Remote Sensing

[12] Because concurrent in situ measurements along the tracks of the hurricanes we examined were not available, satellite data are used in this study. These data include SST, as derived from the Advanced Very High Resolution

Radiometer (AVHRR) onboard certain NOAA satellites, and chl-a, as derived from the SeaWiFS sensor onboard the Orbital Sciences Corporation's OrbView-2 satellite [McClain, 2001]. Details of these satellites and their data are provided in Appendix A.

[13] To obtain representative SST and chl-a values along each hurricane track, the following procedure was used. First, chl-a pixel values within the box greater than 60 mg m^{-3} were set to zero and the SST pixel values within the box were checked for obvious errors. For the NHC-determined latitude and longitude for each hurricane track point within

the box, a “cell” was constructed that extended 0.5° latitude north and south and 1° longitude west and 2° longitude east of this track point. The SST or chl-a values for each pixel within this cell were summed and divided by the number of nonzero pixels (to minimize the impact of any cloudy pixels possibly remaining in the chl-a 8-day means or SST 7-day composites). As these numbers are calculated for each point along the hurricane track within the box, they are summed. The final chl-a or SST along-track value representing each hurricane is then divided by the number of track points within the box. The number of track points within the box depends on the forward speed of the hurricane and how frequently the NHC issued hurricane advisories (every 6 hours and more often when populated land was being threatened). Such an SST or chl-a value is then determined for each 7-day composite AVHRR image or 8-day mean SeaWiFS image, respectively, for data along the entire hurricane track within the box defined above, beginning several weeks before hurricane passage to a month or more after hurricane passage. In this way, we have determined representative along-track SST and chl-a values before (as a benchmark for seasonal and interannual variability at a given location) and after each hurricane as it passes through the box. Details of this method will be illustrated for 1998 Hurricane Bonnie in section 3.

2.2. Parameters Derived From National Hurricane Center (NHC) Reports

[14] Because in situ meteorological measurements were not available, we obtained the physical parameters of the hurricanes from NHC reports, including the hurricane track (latitude, longitude), the maximum sustained winds, the transit speeds, the radii of hurricane-force winds, and the radii of tropical storm force winds. While each hurricane was within the box defined above, we then determined the maximum of its reported maximum sustained wind speeds, the mean of its reported maximum sustained wind speeds, the maximum of its reported radii of hurricane-force winds and the maximum of its reported radii of tropical storm force winds. The transit time of each hurricane within the box was determined by taking the NHC reported times for each track point within the box and calculating the time difference between the track’s endpoints within the box. The transit distance of each hurricane within the box was determined by summing the distances between each track point within the box. The transit speed of each hurricane within the box was then calculated as this transit distance divided by the transit time.

[15] Using the NHC-reported physical parameters described above, we estimated certain derived parameters used in other hurricane studies [e.g., *Greatbatch*, 1984; *Price et al.*, 1994; *Dickey et al.*, 1998b]. These parameters include the alongtrack scale L_i , the nondimensional storm speed S , the Mach number C , and the isopycnal displacement of the seasonal thermocline η . The equations for the along-track scale and nondimensional storm speed are

$$L_i = U_H/f \quad (1)$$

$$S = \pi U_H/4fR, \quad (2)$$

where U_H is the hurricane transit speed, f is the Coriolis parameter, and R is the radius to maximum stress. As an

estimate for R , we used the NHC-reported radius of hurricane-force winds. The value of S is considered an indication of the timescale over which the ocean experiences the wind stress of the hurricane compared with the inertial period and thereby an indication of hurricane-generated near-inertial ocean response. *Greatbatch* [1984] considered it to be about the same as his k parameter, a ratio of the time during which upwelling occurs to the time over which deep water entrainment occurs. The Mach number is an indication of the degree of hurricane-induced upwelling and is given by

$$C = U_H/c, \quad (3)$$

where c is the gravest mode internal wave phase speed, assumed to have a nominal value of 1.9 m s^{-1} [*Dickey et al.*, 1998b]. The isopycnal displacement of the seasonal thermocline due to storm-induced upwelling is defined by *Price et al.* [1994] as

$$\eta = \tau/(\rho_0 f U_H), \quad (4)$$

where ρ_0 is the water density (we used a nominal value of 1020 kg m^{-3}) and τ is the wind stress calculated from

$$\tau = \rho_a(0.49 + 0.065U_{10}) \times 10^{-3}U_{10}^2, \quad (5)$$

where ρ_a is the air density (we used a nominal value of 1.26 kg m^{-3}) and U_{10} is the maximum wind speed of the hurricane.

2.3. Parameters Derived From National Ocean Data Center 1998 Atlas

[16] Because we do not have in situ oceanographic measurements during hurricane passage, we attempted to estimate the effects of hurricane-induced upwelling entrainment by deriving seasonal thermocline and nitracline depths from climatological data. The resulting estimates were compared with our satellite observations in an effort to learn whether the observed post-hurricane chl-a increase could be consistent with a phytoplankton bloom initiated by the entrained nutrients. For this climatological data, we used the NOAA National Ocean Data Center (NODC) 1998 World Ocean Atlas, which includes seasonal nitrate profiles down to various depths [*Conkright et al.*, 1998]. The values in this atlas are objectively analyzed 1° squares at standard depths that are interpolated from actual profile measurements made at different times and locations over a number of years. For temperature, there is a profile for each month at each integer latitude and longitude at standard depths. For nitrate, there is a profile at each integer latitude and longitude and these profiles are organized into trimonthly blocks according to season (e.g., January, February, and March are winter) because there are fewer data for nutrients. In our analysis, we used the seasonal nitrate values at the NODC-defined standard depths down to 300 m (i.e., 0, 10, 20, 30, 50, 75, 100, 125, 150, 200, 250, and 300 m depths). Note that while limited numbers of chl-a profiles were available from NODC, they were not used in our analysis because they were annual means that only extended to depths of 100 m.

[17] For each hurricane track point within the box, the NODC profile values at the closest NODC grid point (i.e.,

Table 1. Hurricane Physical Characteristics With Satellite-Derived SST and chl-a Responses

Storm	Wind Speed, (m s ⁻¹)		Transit Time, hours	Transit Distance, km	Transit Speed, km hr ⁻¹	Radius Max Winds, km		Chl-a, mg m ⁻³		SST, °C	
	Max	Mean				Tropical Storm Force	Hurricane Force	Before	After	Before	After
1998 Bonnie	51	45	114	2032	18	370	232	0.0685	0.0915	30.3	28.2
1998 Danielle	45	39	120	2527	21	325	150	0.0711	0.0875	29.5	28.3
1999 Cindy	63	54	42	634	15	370	140	0.0456	0.0551	30.6	28.0
1999 Dennis	47	32	123	1570	13	350	185	0.0668	0.0772	30.9	29.8
1999 Floyd	69	59	102	2113	21	370	220	0.0730	0.0909	30.4	28.8
1999 Gert	63	55	96	1529	16	415	220	0.0596	0.0817	29.6	27.6
1999 José	34	29	54	1331	25	220	55	0.0590	0.0620	28.9	28.4
2000 Alberto	38	36	18	465	26	280	110	0.0489	0.0555	29.4	28.5
2000 Florence	34	26	108	1238	12	280	35	0.0596	0.0975	29.0	28.2
2000 Isaac	58	56	12	390	32	370	95	0.0476	0.0907	29.1	27.0
2000 Michael	34	27	36	277	8	140	35	0.0759	0.1364	27.6	25.8
2001 Erin	47	28	63	1214	19	230	75	0.0525	0.0565	30.0	29.7
2001 Michelle	38	35	30	1295	43	465	230	0.1278	0.1513	28.0	25.4

integer latitude and longitude) were identified. Only those NODC profiles without any missing or zero nitrate values between the surface and 300 m depth were used. As we did for the satellite-derived SST and chl-a data, we used values from NODC grid points within a cell defined for each hurricane track point as follows. For each track point, each cell extends 2° longitude to the right and 1° longitude to the left of the hurricane track and is also bounded by latitudes a half degree north and south of each hurricane track point.

[18] For each hurricane, we took each along-track NODC profile and determined the slope between each pair of NODC-defined standard depths. The depths at the top of the maximum slopes of nitrate were called the nitracline depths for each NODC grid point along the hurricane track. The mean of these depths for each hurricane then became the nitracline depth for that storm. It should be kept in mind that these depth estimates are rather coarse because of the large differences between the NODC standard depths, especially below 50 m. Finally, storm impact on the nitracline was estimated by combining this NODC-based climatological nitracline depth with the estimate of thermocline displacement (η) described earlier.

3. Remote Sensing Observations

[19] Table 1 provides a summary of hurricane characteristics and our remote sensing observations for the hurricane seasons of 1998–2001. In the following subsections, we summarize each hurricane season as it affected the Sargasso Sea. The hurricane tracks for each of these years are overlaid on example SST images from each season in Figures 1 and in Figures 6–8 in sections 3.2–3.4.

3.1. 1998 Hurricane Season

[20] According to the NHC, the 1998 Atlantic hurricane season was more active than usual. It was the first complete season in which SeaWiFS made observations and produced two hurricanes (Bonnie and Danielle) that crossed the Sargasso Sea (Figure 1). The SST image in Figure 1 was selected as an example illustration because it shows the SST around the time Bonnie and Danielle crossed the box.

[21] Bonnie was the first hurricane of the season, originating from a large and vigorous tropical wave that moved off the coast of Africa. Bonnie entered the box (Figure 1) on

21 August as a tropical storm with maximum sustained winds of 22 m s⁻¹ and a forward speed of about 10 m s⁻¹. By 23 August, Bonnie had intensified into a major hurricane with maximum sustained winds of 51 m s⁻¹. At the same time, its forward motion slowed to less than 3 m s⁻¹. During 24 August, its forward motion slowly increased to about 4 m s⁻¹. Because of its horizontal extent, Bonnie disturbed a large area of ocean and presented a considerable threat as it accelerated toward the coast at almost 7 m s⁻¹ on 25 August. Bonnie's winds decreased to 38 m s⁻¹ and its forward motion decreased to less than 5 m s⁻¹ as Bonnie's eye crossed the Carolina coast on 26 August.

[22] We now illustrate the method of determining pre-storm and post-storm chl-a and SST values using Bonnie as an example. We used several satellite images of SST and chl-a, beginning a couple of weeks before storm passage to weeks or months following storm passage, depending on when the chl-a values returned closest to their pre-storm values. For example, comparing the satellite images of undisturbed SST and chl-a (Figures 2a and 2b, respectively) with those following the passage of Bonnie (Figures 3a and 3b), an increase in the near-surface chl-a appears along the storm track in the same vicinity as the cool wake resulting from the induced mixing and upwelling. Recall that this region of the North Atlantic is typically oligotrophic so that chlorophyll concentrations in this area are rather low. Therefore the chl-a scale used in these SeaWiFS images is linear with the scale maximum deliberately set to a low value to emphasize the features shown in the Sargasso Sea. This means that chl-a concentrations greater than the maximum value on this scale will be indistinguishable from the scale maximum and chl-a concentrations should not be determined for coastal regions from these images. This scaling limit was only used to produce the images in Figures 2b and 3b in order to emphasize the chl-a wake left by Bonnie and was not imposed when the subsequent chl-a calculations were made.

[23] The along-track spatially averaged 8-day mean chl-a concentrations within the box defined above were determined, as described in section 2, for nine contiguous 8-day periods between 5 August and 16 October. A time series of the resulting chl-a over seven of these contiguous 8-day periods is shown in the top panel of Figure 4, with the time during which Bonnie was in the box shown by the

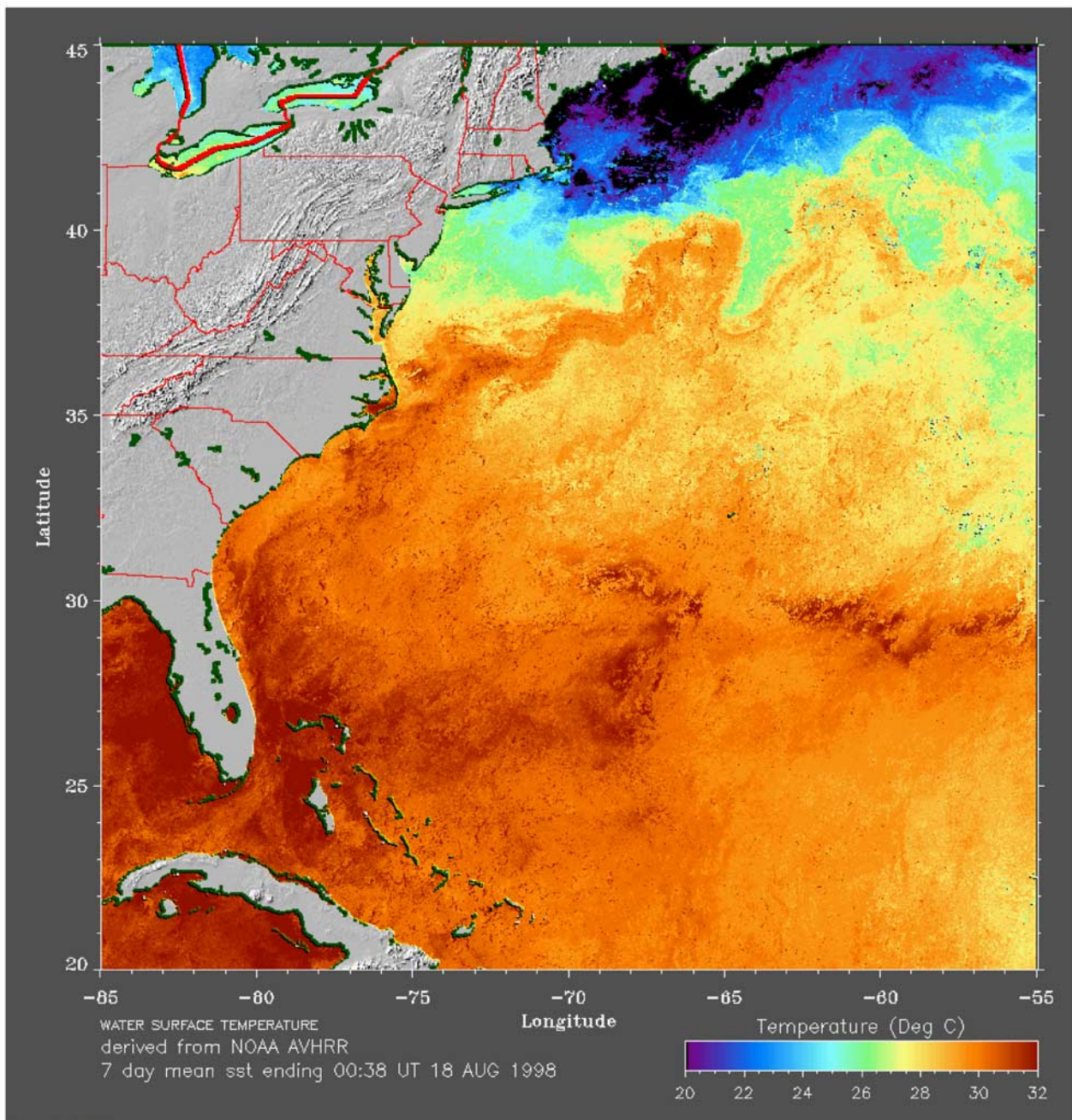


Figure 2a. The 7-day composite sea surface temperature data acquired 18 August 1998 from NOAA-12 and NOAA-14, before the passage of Bonnie.

vertical dashed lines. For the 21–28 August period, Bonnie’s presence within the box during 21–26 August raised the 8-day mean chl-a concentration along its track by about 34% (an increase of about 0.023 mg m^{-3}) from the previous 8-day period. During the 29 August to 5 September and 14–21 September periods, this mean fell very slowly, although at least some of this effect may be because Hurricane Danielle crossed Bonnie’s path during 26–31 August. In fact, Danielle entered the box near its southeast corner about 21 hours after Bonnie left the box near its northwest corner (Figure 1). Bonnie exited our box on 26 August, but it wasn’t until the 8-day period beginning

8 October that the along-track averaged 8-day mean surface chl-a level returned to a level closest (within 3.5%) to the pre-Bonnie level.

[24] The lower half of Figure 4 shows the time series SST response to Bonnie along the track in the same way that the along-track chl-a values were determined. This 7-day composite SST decreased by about 2°C (about 6.9%) following passage of this storm. Later this SST increased toward its pre-storm values. Time series of SST and chl-a such as these were used to determine the SST and chl-a before and after each hurricane. The pre-hurricane values were those before the hurricane entered the box, while the post-hurricane

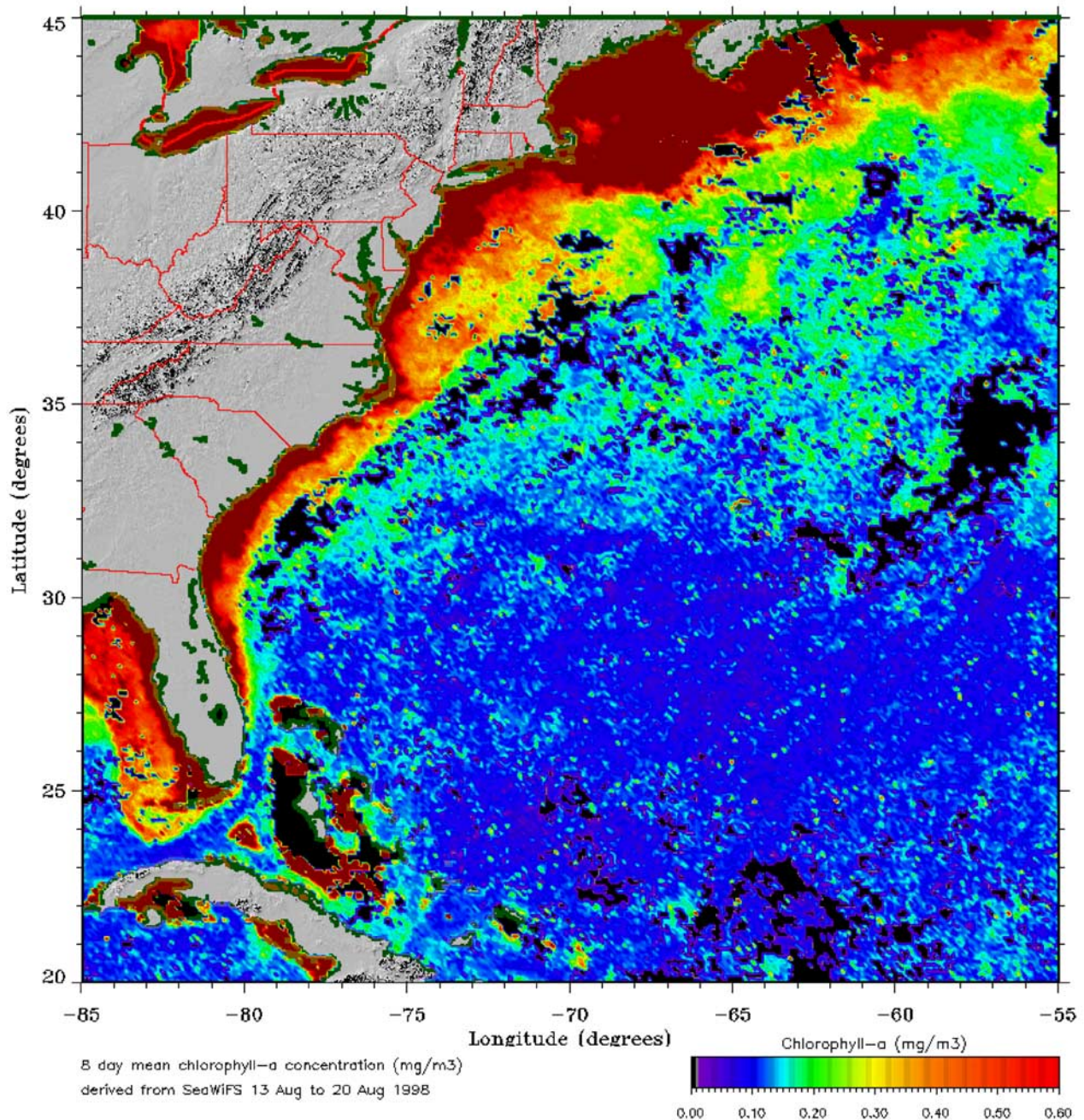


Figure 2b. The 8-day mean chlorophyll concentration acquired 20 August 1998 from SeaWiFS. The black pixels are due to clouds. The color scale is deliberately set to have a low maximum value in order to enhance the Sargasso Sea features.

values were those while the hurricane was within the box or just after it left the box. Note that the peak post-Bonnie 8-day mean chl-a pixel value (1.135 mg m^{-3}) during this same time period is much larger than the peak post-Bonnie averaged value shown in Figure 4 and Table 1, with the difference being that this larger value was not spatially averaged over the area within 1° longitude to the left and 2° longitude to the right of the hurricane track located within the box. Because this maximum pixel value occurred only three times in the post-Bonnie chl-a image, a histogram was plotted in Figure 5 to illustrate the frequency distribution of

the pre-Bonnie and post-Bonnie nonzero pixel values. Note, that if the most frequent chl-a pixel values were used, the post-Bonnie chl-a increase would be about 62.5%.

[25] Danielle became a hurricane on 25 August, after originating from a tropical wave that moved off the west coast of Africa and became a tropical depression near the Cape Verde Islands. It entered the box in Figure 1 on 26 August with maximum sustained winds of 40 m s^{-1} . Danielle then weakened to 33 m s^{-1} as it crossed Bonnie's cool wake on 29 August. Hurricane-induced surface cooling is known to influence the strength of subsequent hurricanes

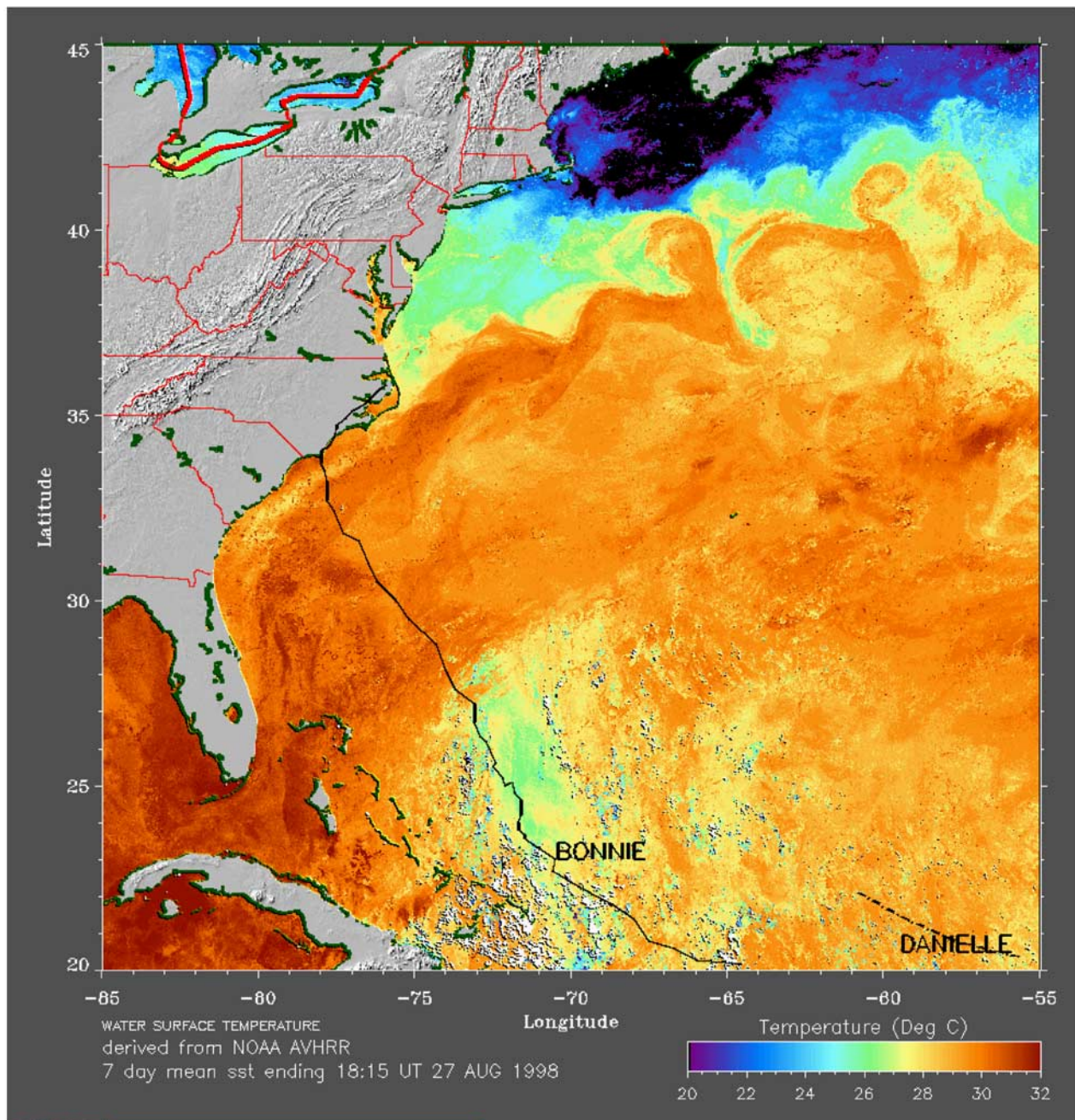


Figure 3a. The 7-day composite sea surface temperature acquired 27 August 1998 from NOAA-12 and NOAA-14. Tracks of Bonnie and Danielle are shown up to their positions on 27 August 1998.

crossing their cool wake [Brand, 1971; Anthes and Chang, 1978] and even the strength of the parent storm due to the reduced energy supply associated with cooler waters [Black and Holland, 1995]. While Danielle exited the box on 1 September, it wasn't until the 8-day period beginning 14 September that the spatially averaged 8-day mean surface chl-a value fell to a value close to, and actually just below, its pre-storm value.

3.2. 1999 Hurricane Season

[26] According to the NHC, the 1999 Atlantic hurricane season was slightly above average in number, with eight

hurricanes compared to a long-term seasonal average of six. Although there are no major hurricanes in a typical season before the end of August, there had been two major hurricanes by that time in 1999. The 1999 season was further remarkable in that it had the largest number of Saffir-Simpson Category 4 (wind speeds $58\text{--}69\text{ m s}^{-1}$) hurricanes in a single season since 1886, according to the NHC. The hurricanes that entered our box during 1999 were Cindy, Dennis, Floyd, Gert, and José (Figure 6). The SST image from 16 September is used to illustrate this season because it shows the SST near the times most of the hurricanes were in or near the box.

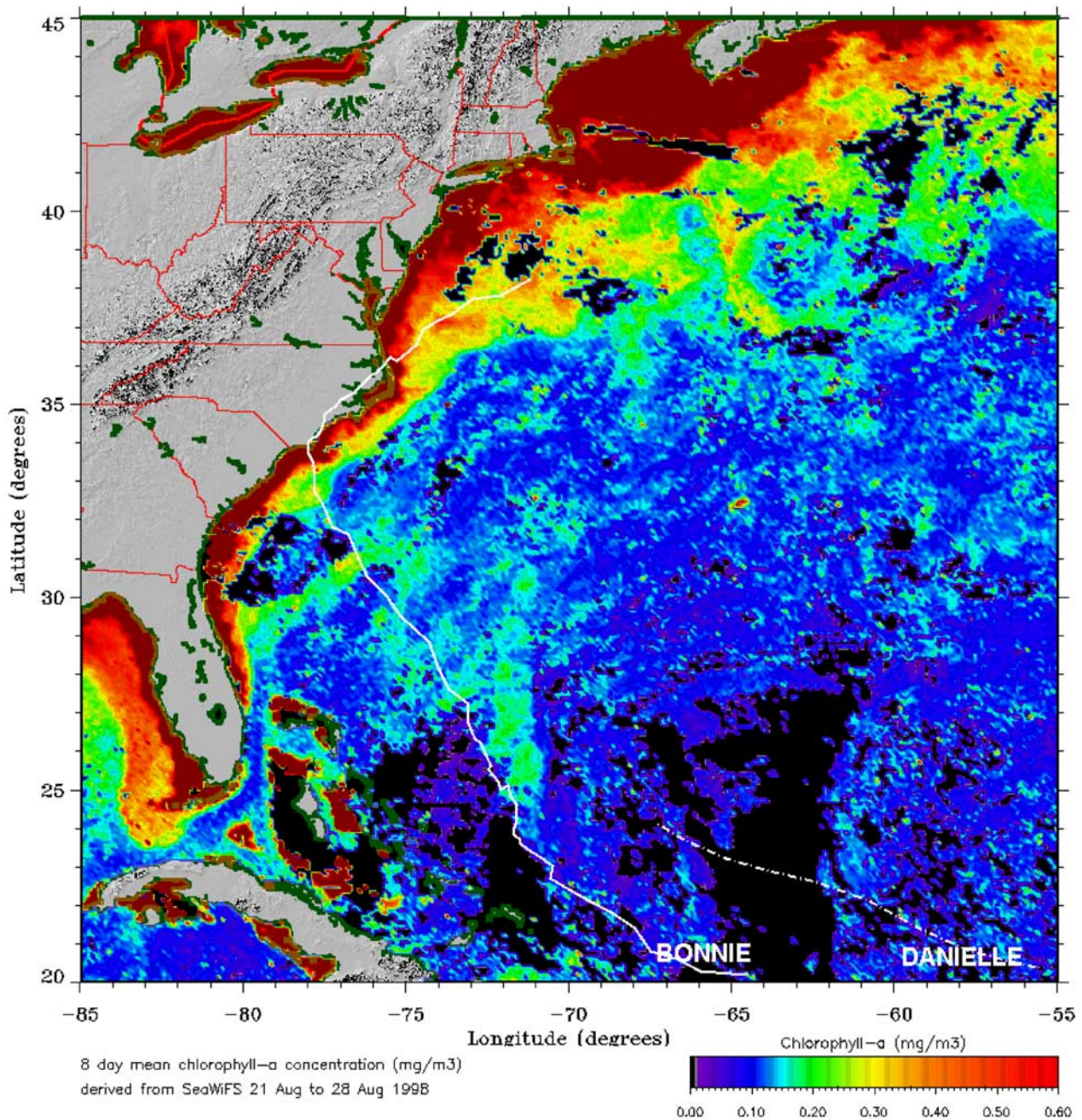


Figure 3b. The 8-day mean chlorophyll concentration acquired 28 August 1998 from SeaWiFS. Tracks of Bonnie and Danielle are shown up to their positions on 28 August 1998. The black pixels are due to clouds. Note explanation of color scale in Figure 2b.

[27] Cindy originated from a tropical wave that exited the west coast of Africa and became a tropical depression near the Cape Verde Islands. Cindy was the first major hurricane of the season and entered our box from the southeast on 27 August with 40 m s^{-1} winds that increased to 63 m s^{-1} before Cindy exited the box to the northeast on 29 August. On 28 August, Cindy absorbed Tropical Storm Emily (maximum sustained winds 16 m s^{-1}), which may have had an effect on upwelling. When spatially averaged along its track, the 7-day composite SST's decreased by about 2.6°C (8.5%) following Cindy's passage, while the 8-day

mean chl-a increased by about 21% from 0.0456 mg m^{-3} for 21–28 August to 0.0551 for 29 August–5 September. Of the 13 hurricanes we examined, Cindy had the lowest pre-passage surface chl-a value. After Cindy exited the box on 29 August, the along-track surface chl-a value fell to a value closest to its pre-hurricane level for the 8-day period beginning 30 September.

[28] Dennis originated from a tropical wave that moved off the African coast and became a tropical depression near Turks Island north of Hispaniola. Dennis developed into a tropical storm with 16 m s^{-1} winds within our box on

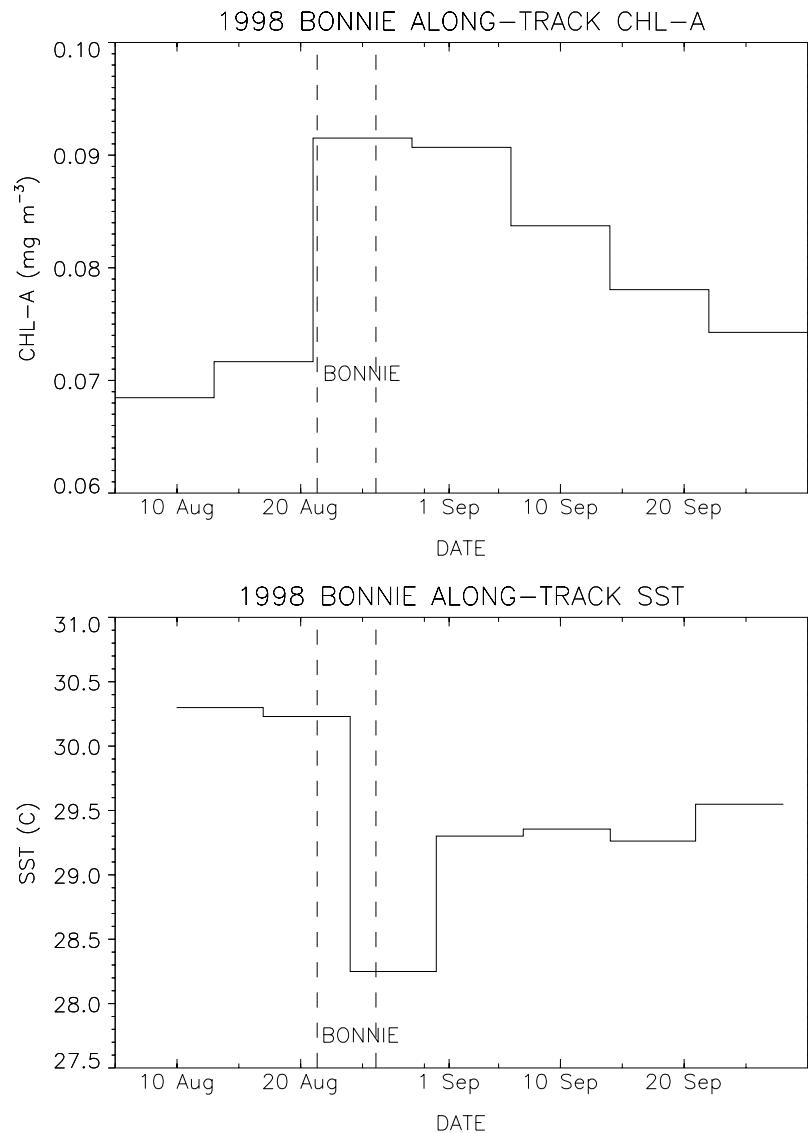


Figure 4. SeaWiFS-derived mean chlorophyll and AVHRR-derived mean SST from the along-track region along the part of Bonnie's path described in the text.

24 August and became a hurricane on 26 August. It exited the box on 29 August as a hurricane with 47 m s^{-1} winds. Of the 13 storms examined, Dennis was one of slower moving storms (about 13 km hr^{-1}). The along-track spatially averaged surface chl-a value returned to a value closest to (within about 2%) its pre-Dennis value for the 8-day period beginning 6 September.

[29] Floyd originated from a tropical wave that emerged from Africa and became a tropical depression east of the Lesser Antilles. Floyd entered our box as a hurricane with 36 m s^{-1} winds in the afternoon of 10 September. It strengthened with winds of 69 m s^{-1} on 13 September, perhaps as a result of crossing the very warm patch of water (seen near the "F" in Floyd on Figure 6). It maintained that strength for about 24 hours before the winds decreased to about 63 m s^{-1} as it exited the box on 15 September. Floyd was faster than Dennis and moved at about 21 km hr^{-1} . After exiting the box on 15 September, the averaged along-track surface chl-a value fell to closest to its pre-storm value (within about 6%) for the 8-day period beginning 8 October.

[30] Of the 1999 storms examined, only Dennis and Floyd crossed each other's tracks. Recall that in 1998, Bonnie and Danielle crossed each other's tracks also. The change in chl-a and SST associated with Dennis (about a 16% increase and 4% drop, respectively) was less than that with Bonnie (about a 34% increase and 7% drop, respectively). However, the change in chl-a and SST associated with Floyd (25% increase and 5% decrease, respectively) was close to that with Danielle (23% increase and 4% decrease, respectively). In 1998, the more powerful storm (Bonnie) preceded the weaker storm. In 1999, the more powerful storm (Floyd) followed the weaker storm. There was over a week gap between Dennis' exit and Floyd's entering the box while there was less than a 24-hour gap in time between when Danielle and Bonnie were within the box. In addition, the tracks of Dennis and Floyd were much closer to the U.S. coast where both SST and chl-a were already higher prior to the influence of these storms.

[31] Gert originated from a tropical wave that developed into a tropical depression in the far eastern North Atlantic

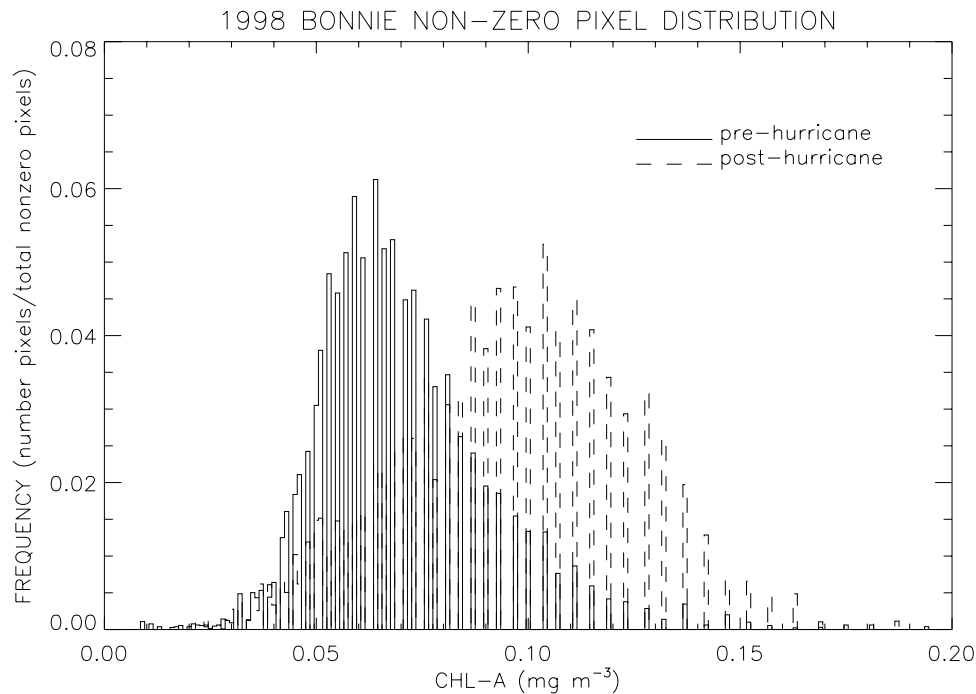


Figure 5. Frequency distribution of non-zero pixels in the pre-Bonnie and post-Bonnie chl-a images. The ordinate is the number of non-zero pixels with values of chl-a within the 0.001 mg m^{-3} bin shown on the abscissa. These pixel values were along Bonnie's track through the box defined in the text. Because the fraction was near zero above 0.2 mg m^{-3} , only those chl-a bins below that value are plotted. For those nonzero pixels equal to or greater than 0.2 mg m^{-3} , the pre-Bonnie and post-Bonnie images contained 1.6% and 5.9% of the total nonzero pixels, respectively.

Ocean. Gert entered the southeast corner of the box as a hurricane with 63 m s^{-1} winds on 17 September. Once inside the box, it slowly weakened until it exited the box on 21 September with 49 m s^{-1} winds. The along-track spatially averaged 8-day mean surface chl-a fell to a value closest to its pre-storm value for the 8-day period beginning 16 October. The largest along-track area-averaged increase in chl-a (37%) in 1999 occurred with Hurricane Gert. However, Gert had the second largest SST decrease (6.8%), compared with the largest SST decrease (8.5%) for Cindy, for the 1999 season. While Gert and Cindy were within the box, their maximum wind speeds were the same (63 m s^{-1}) and their mean wind speeds were almost the same (a difference of only 1 m s^{-1}). The different chl-a response to SST decrease between these storms may be due to the fact that Gert was a larger storm and spent more time inside the box (i.e., Ekman pumping was probably more pronounced) than Cindy.

[32] José originated from a tropical wave that exited the African coast and became a tropical depression between Africa and the Lesser Antilles. José became a tropical storm on 17 October and strengthened to a hurricane on 19 October. After its winds reached 45 m s^{-1} on 20 October, it weakened to a tropical storm on 21 October. It then entered the box on 22 October as a tropical storm (29 m s^{-1} winds). It weakened further to 27 m s^{-1} winds on 23 October before re-intensifying and leaving the box as a hurricane (34 m s^{-1} winds) on 24 October. The area-averaged chl-a increased from 0.0590 mg m^{-3} to 0.0620 mg m^{-3} after José left the box and continued to

increase, reaching 0.0806 mg m^{-3} by the end of November (we did not collect SeaWiFS chl-a values after 30 November). Note that we always chose values for post-storm chl-a peaks that occurred no later than about a week after hurricane passage, in order to be more certain that these increases were associated with a particular storm. Of the 13 storms studied, José had the smallest increase in along-track chl-a (both absolute value and percent). Although its SST response was weak (0.54°C), it was not quite as weak as 2001 Erin. José was the smallest and had the weakest winds of the five 1999 storms we examined.

3.3. 2000 Hurricane Season

[33] The 2000 Atlantic hurricane season was also above average, both in the number of tropical storms and in the number of hurricanes (eight compared to a typical season of six), according to the NHC. Interestingly, there were no hurricane landfalls in the United States during this season [Elsner, 2003]. Four hurricanes (Alberto, Florence, Isaac, and Michael) entered our box (Figure 7). Alberto and Isaac were among the strongest of the season.

[34] Hurricane Alberto made the NHC record as the third longest-lived tropical cyclone in the Atlantic. It formed off the African coast on 3 August, became a hurricane on 5 August, weakened to a tropical storm on 9 August, but regained hurricane strength on 10 August. It entered our box on 9 August with 31 m s^{-1} winds and exited on 11 August with 38 m s^{-1} winds, never moving farther west than about 58.7°W longitude. The along-track spatially averaged 8-day mean chl-a concentration returned to a

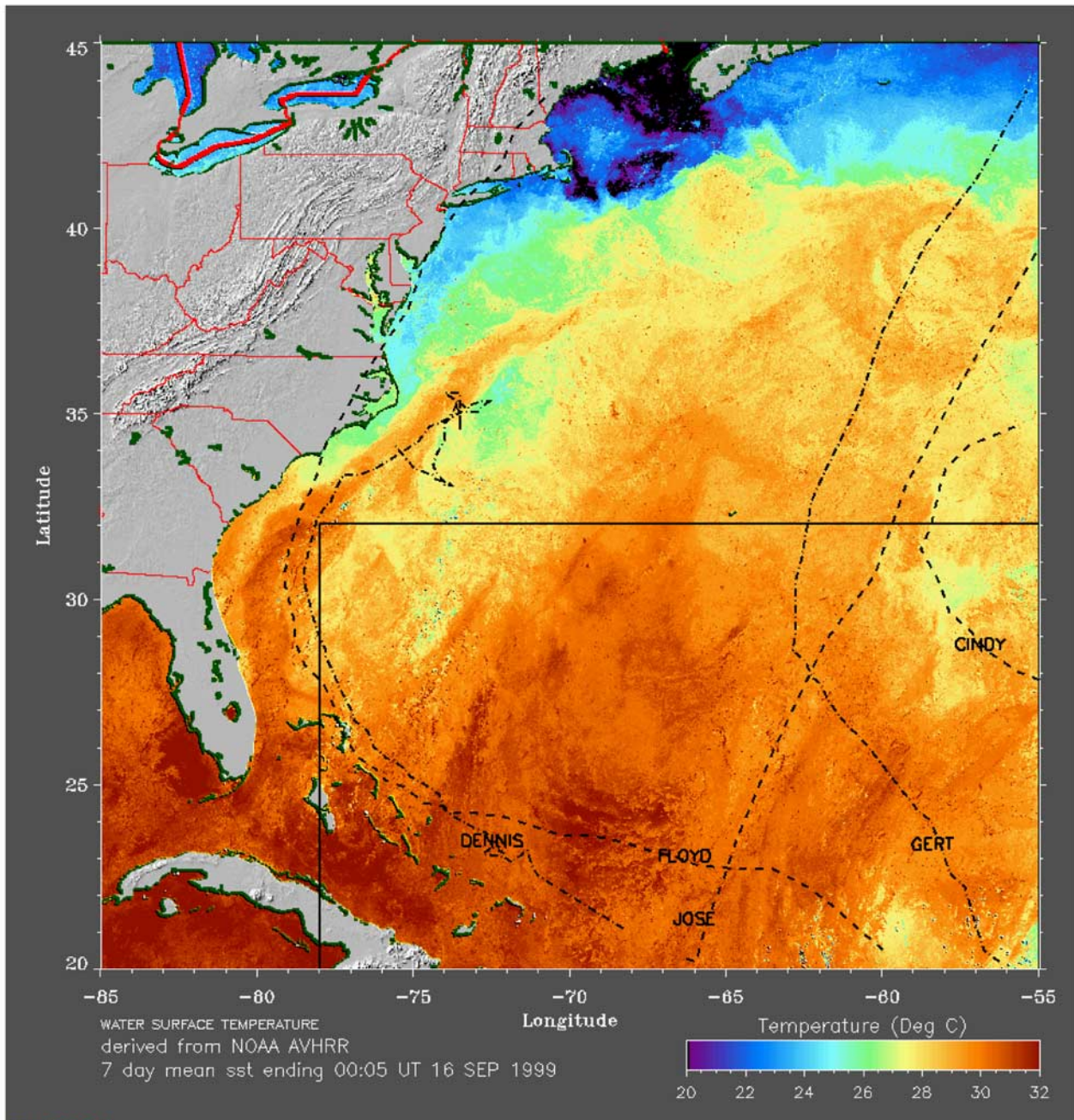


Figure 6. The 7-day composite sea surface temperature data acquired 16 September 1999 from NOAA-12 and NOAA-14. The box defined in the text is outlined. The tracks of the 1999 hurricanes discussed in the text are superimposed.

value closest to its pre-Alberto level for the 8-day period beginning 13 September.

[35] Florence originated from a subtropical depression associated with a cold front that had moved off the U.S. east coast during the first week in September and become stationary over the western North Atlantic. Florence acquired tropical characteristics and was classified as a tropical depression within our box on 11 September and strengthened to a hurricane on 12 September. It quickly weakened to tropical storm strength on 13 September. While it remained within our box for about 108 hours, it was a hurricane (34 m s^{-1} winds) for less than 24 hours. Its

forward motion made it one of the slowest hurricanes in our study. The maximum radius of hurricane-force winds was only 35 km. After Florence left the box on 16 September, the along-track spatially averaged 8-day mean chl-*a* fell to a value closest to its pre-storm level for the 8-day period beginning 21 September.

[36] Isaac originated from a strong tropical wave that emerged from the western African coast and became a tropical depression near the Cape Verde Islands. Isaac entered our box on 29 September with 58 m s^{-1} winds and quickly exited the box about 12 hours later the same day with 54 m s^{-1} winds. Isaac was the strongest storm

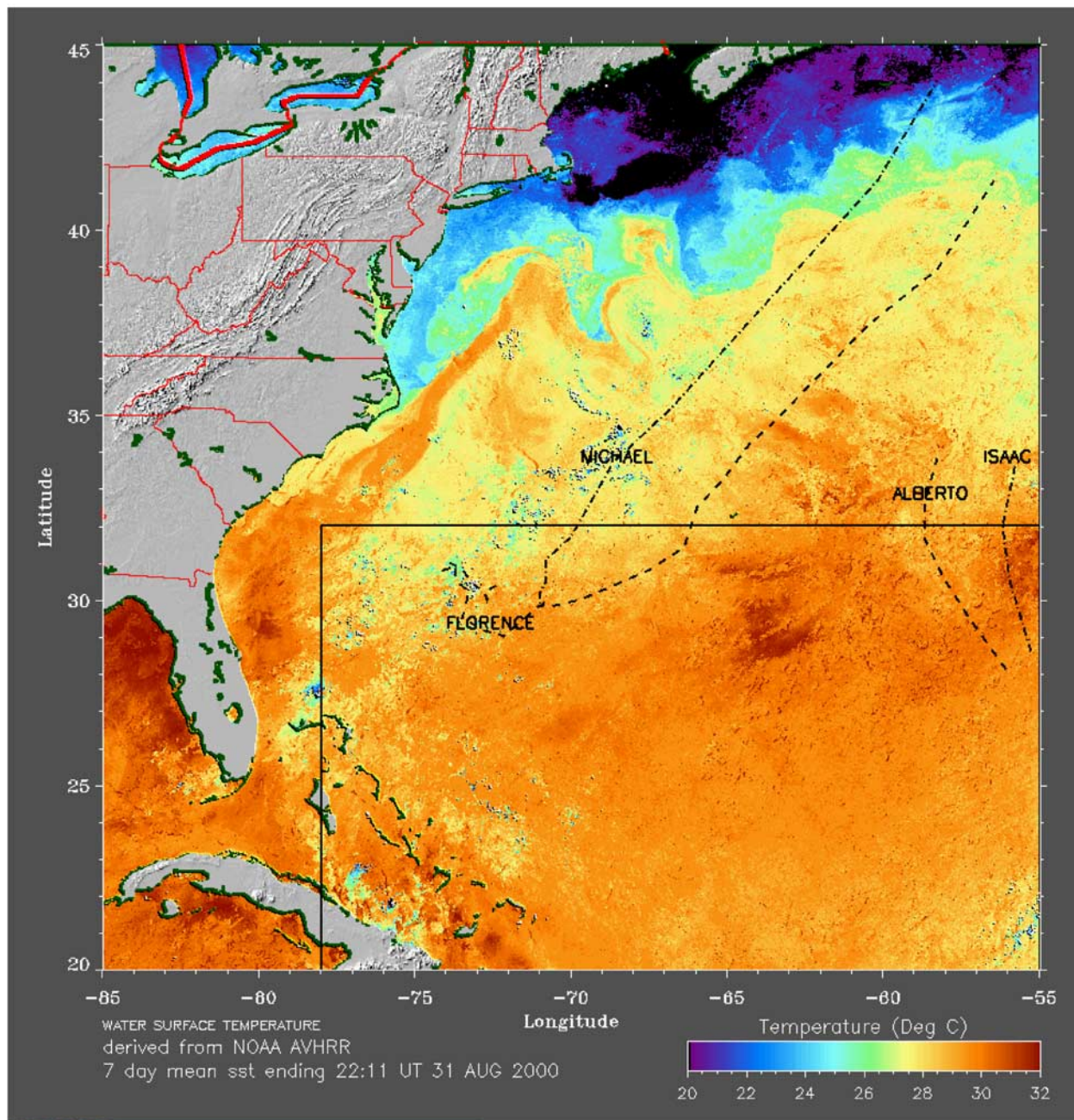


Figure 7. The 7-day composite sea surface temperature data acquired 31 August 2000 from NOAA-12 and NOAA-14. The box defined in the text is outlined. The tracks of the 2000 hurricanes discussed in the text are superimposed.

(58 m s^{-1} winds) and had the largest maximum tropical storm force wind radius (370 km) of any of the year 2000 storms we studied. In contrast, the radius of its hurricane-force winds was only 95 km. For the 2000 season, it was the fastest moving storm and had the largest along-track SST decrease (2.1°C). It had the largest chl-a increase (91%) of all 13 hurricanes. After Isaac left the box on 29 September, the along-track area averaged chl-a returned to a value closest to its pre-storm level for the 8-day period beginning 15 October.

[37] Like Florence, Michael had its origins from a sub-tropical depression associated with a cold front that had moved off the southeast U.S. coast on 7 October and became stationary over the western North Atlantic. Michael acquired tropical characteristics and was classified as a tropical storm on 17 October while it was within our box. It became a hurricane (34 m s^{-1} winds) later that same day. It exited the box on 18 October about 36 hours after it formed. Although Michael was a small and weak storm, it had the second largest increase in along-track chl-a

(about 80%) of any of the 13 storms we studied. It had almost the largest decrease in SST for the year 2000. One explanation may be that it was the slowest moving storm of all 13 studied, with a mean forward motion of only 7.7 km hr^{-1} . The next slowest was Florence at 11.5 km hr^{-1} . After Michael exited the box on 18 October, the along-track area-averaged chl-a fell from its peak value of 0.1364 mg m^{-3} to 0.1190 mg m^{-3} but then alternately rose and fell between about 0.14 and 0.12 mg m^{-3} through the end of November (we did not analyze SeaWiFS data beyond the end of November).

3.4. 2001 Hurricane Season

[38] The 2001 Atlantic hurricane season was also a very active one, with nine hurricanes (compared with six in an average season), four of them major. All the storms that eventually became hurricanes formed during September through November. Interestingly, three of these formed during November, which was an NHC record for that month, and two of these were major hurricanes. For this season, only Hurricanes Erin and Michelle were well within the box (Figure 8).

[39] Erin originated from a tropical wave that had emerged off the African coast and became a tropical depression near the Cape Verde Islands on September 1. Erin became a tropical storm on 2 September, dissipated on 5 September, and then re-formed on 6 September. It entered our box that same day with 16 m s^{-1} winds and became a hurricane on 8 September. The winds increased to 47 m s^{-1} by the time it exited our box on 9 September. The along-track spatially averaged 8-day mean chl-a value returned to a value closest to its pre-Erin level for the 8-day period beginning 22 September. The maximum along-track 8-day mean chl-a pixel was 0.389 mg m^{-3} , compared with the along-track area-averaged chl-a of 0.0565 mg m^{-3} in Table 1.

[40] Michelle originated from a tropical wave that emerged off the African coast but did not develop into a tropical depression until it was off the coast of Nicaragua on 29 October. Michelle became a hurricane on 2 November and entered our box on 5 November with 38 m s^{-1} winds. The winds weakened to 34 m s^{-1} later the same day. On 6 November, the winds returned to 38 m s^{-1} but weakened to minimal hurricane force (34 m s^{-1}) by the time it exited our box later that same day. After exiting the box on 6 November, the along-track area-averaged chl-a returned to a value closest to its pre-Michelle level for the 8-day period beginning 9 November. The maximum along-track 8-day mean chl-a pixel was 3.802 mg m^{-3} , compared with the along-track area-averaged chl-a of 0.151 mg m^{-3} in Table 1. Michelle had the fastest transit speed of any of the storms we studied. It was weaker than Erin but had the greater effect on both chl-a increase and SST decrease. One reason may be because it was more than twice as large as Erin while within the box and therefore affected a much greater area.

4. Analysis and Discussion

[41] Each of the years 1998 through 2001 saw higher than normal hurricane activity for the Atlantic basin. Of the 13 hurricanes that entered our box during these years, five each occurred in the months of August and September, two

occurred in October, and one occurred in November. We found a post-hurricane increase in chl-a and a decrease in SST for all the hurricanes we studied (Table 1). The post-storm peak chl-a pixel values were always larger than the along-track area mean chl-a values derived as per section 2, indicating that these means may underestimate the peak chl-a response to a hurricane.

[42] Figure 9 shows a consistent SST decrease and chl-a increase following hurricane passage that demonstrates a nearly linear relationship. Each point on the plot is represented by a set of four characters: a lower case letter representing the initial of the month the hurricane was within our box, two numerical digits representing the last two digits of the year, and an upper case letter representing the initial of the storm name (e.g., s99G is 1999 Gert, which was within our box during the month of September). The two hurricanes with the weakest chl-a responses, 1999 José and 2001 Erin, had the smallest SST decreases. Both storms had small hurricane-force wind radii. While Erin had a maximum wind speed about 13 m s^{-1} larger than José, their mean wind speeds were within 1 m s^{-1} of each other.

[43] In addition to the satellite-observed along-track SST decreases and chl-a increases, Table 1 also lists the NHC physical hurricane parameters described earlier. A mostly linear relationship was found between percent chl-a increase and mean wind speed (Figure 10), tropical storm force wind radius, and hurricane-force wind radius. In an effort to quantify the influence of these meteorological parameters on the ocean below, the quantities defined in equations (1)–(5) in section 2 were calculated and are provided in Table 2.

[44] The NODC 1998 Ocean Atlas, which includes a seasonal nitrate climatology, was used to estimate the nitracline depths along the tracks of the hurricanes. For each hurricane, the isopycnal displacement of the seasonal thermocline (η) provides an indication of the effects of Ekman pumping on these nitrate profiles. While we attempted to estimate more directly the post-hurricane nutrient enrichment of the mixed layer, this proved to be highly problematic due to the inherent limitations of the climatological data in relation to the highly episodic and nonlinear nature of these events. Instead, for each hurricane, we added η to the NODC-derived average along-track nitracline depth. Figures 11 and 12 show a similar linear relationship between percent chl-a increase and both a derived hurricane characteristic (S) and a derived measure of oceanic response (nitracline depth plus η).

[45] Most of the 13 hurricanes examined (Figures 9–12) show a similar trend, indicating that storm-induced increases in satellite-observed chl-a could be accompanied by storm-induced increases in surface nitrate concentration due to upwelling and entrainment (e.g., see Figure 11 showing that the pre-storm versus post-storm chl-a differences correlate well with S). This gives us some additional confidence that at least some of the chl-a increase observed overall may be the result of a storm-induced phytoplankton bloom.

[46] It is also interesting to note that the three outliers in the hurricane parameter plots (Figures 9–11) are also outliers in Figure 12: 2000 Florence, 2000 Isaac, and 2000 Michael. When all 13 storms are included, the coefficient of determination (square of the correlation coefficient) is near zero for maximum wind speed and less than 0.12 for tropical and hurricane-force wind radii. The coefficient of

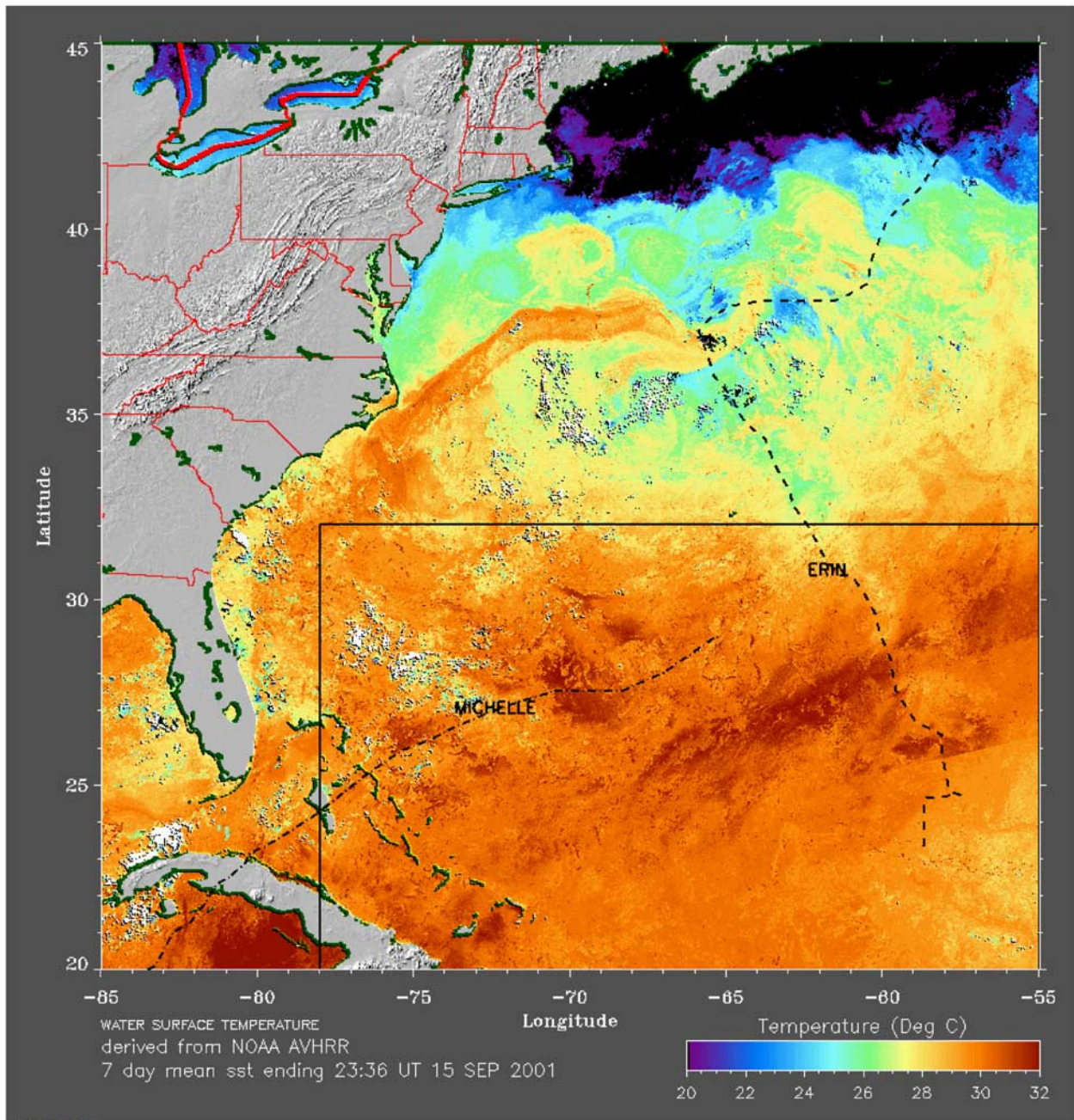


Figure 8. The 3-day composite sea surface temperature data acquired 15 September 2001 from NOAA-12 and NOAA-14. The box defined in the text is outlined. The tracks of the 2001 hurricanes discussed in the text are superimposed.

determination tells us roughly what percent of the variance can be explained by a linear relationship, so a value of 0.12 means that only 12% of the variance can be explained. However, when these three storms are excluded, then maximum wind speed explains 41% of the variance, mean wind speed explains 58% of the variance, tropical storm force wind radius explains 50% of the variance, and hurricane-force wind radius explains 66% of the variance. The transit time explains 25% of the variance, transit distance explains 19% of the variance, and transit speed explains only 6% of the variance.

[47] The percent increases in chl-a with the three outlier storms noted above were much larger than what might be expected based on the observed physical characteristics of the remaining ten storms. Florence and Isaac crossed our box in September, while Michael crossed it in October, so it is not obvious that seasonal effects account for these differences. Isaac, Michael, and Florence had the largest chl-a increases of any of the storms examined (Figure 9), with percent increases of 91, 80, and 64%, respectively. In Table 1, we see that these three storms were also distinguished by their relatively small hurricane-force wind radii.

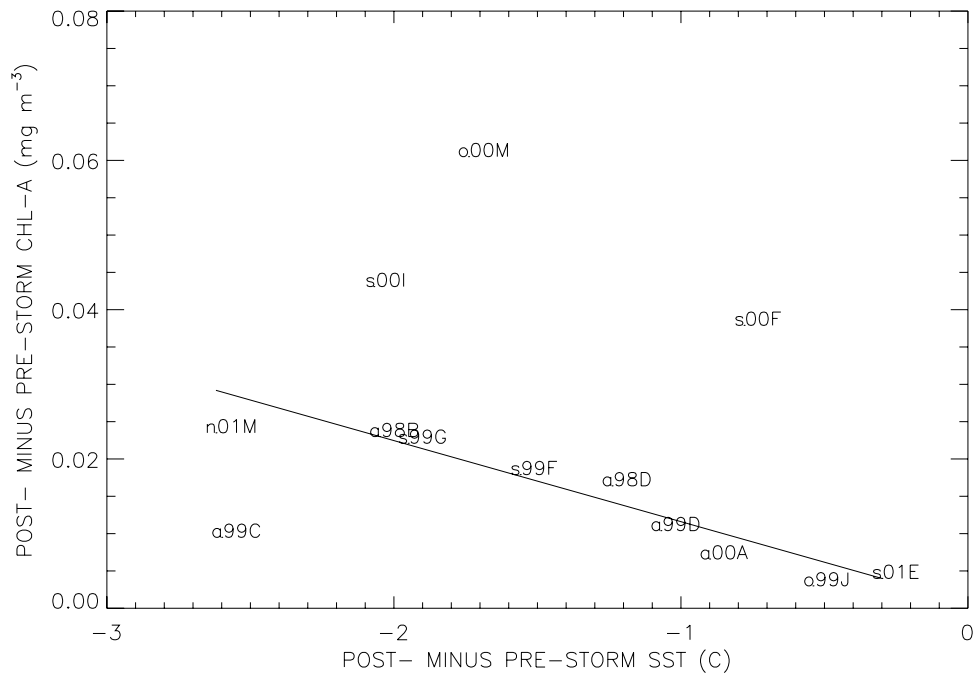


Figure 9. SeaWiFS-derived mean chlorophyll change and AVHRR-derived mean SST change for passage of each of the 13 storms through 20°N, 78°W, 32°N, and 55°W. The labels indicate the first initial of the month the storm was within our box (lower case), the last two digits of the year, and the first initial of the storm name (upper case). The line is a linear least squares fit to all these points.

Florence and Michael were the weakest in terms of mean wind speed and shared the smallest hurricane-force wind radii of all the storms examined. Florence and Michael formed the farthest north of any of the 13 storms examined,

and, unlike the other storms, they originated from subtropical depressions that formed following passage of a cold front from the U.S. east coast into the western North Atlantic. Isaac originated from a tropical wave and formed

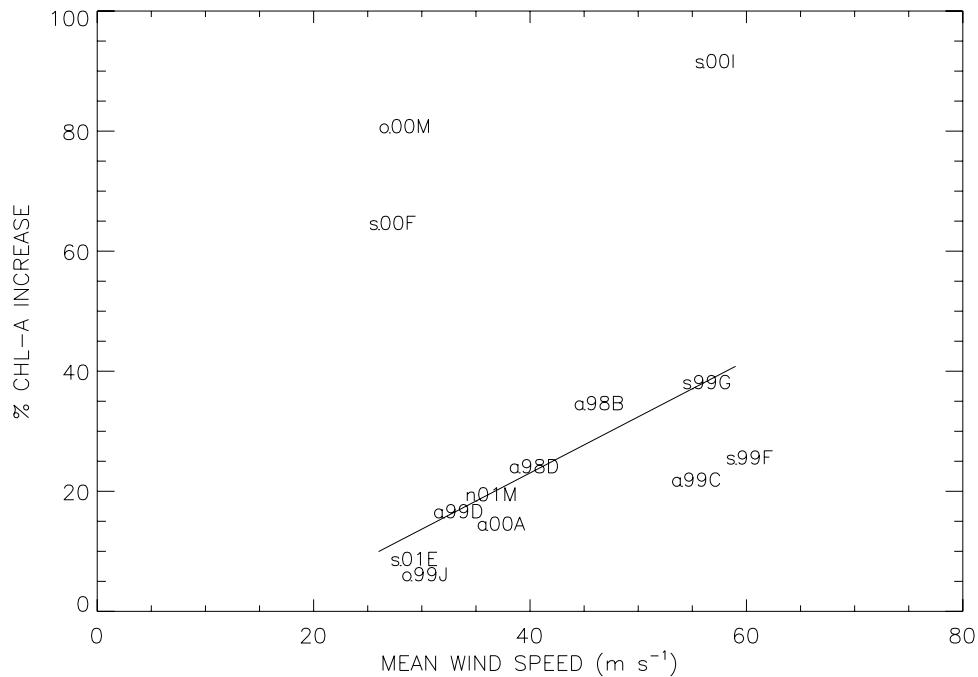


Figure 10. SeaWiFS-derived mean chlorophyll percent change and mean sustained storm wind speed for passage of each of the 13 storms through 20°N, 78°W, 32°N, and 55°W. The labels indicate the first initial of the month the storm was within our box (lower case), the last two digits of the year, and the first initial of the storm name (upper case). The line is a linear least squares fit to all these points.

Table 2. Hurricane Parameters Derived From Equations (1)–(5) With Satellite-Derived SST and chl-a Responses

Storm	τ	L_j , km	S	C	η , m	Number of NHC Track Points Within Box	Dates Within Box	% Change	
								SST	Chl-a
1998 Bonnie	12.47	79.66	0.27	2.6	40.63	38	21–26 Aug.	–6.90	33.60
1998 Danielle	8.71	93.74	0.49	3.08	23.78	21	26 Aug. to 1 Sept.	–4.10	23.10
1999 Cindy	22.93	58.25	0.33	2.21	75.92	8	27–29 Aug.	–8.50	20.80
1999 Dennis	9.87	58.06	0.25	1.87	45.32	40	24–29 Aug.	–3.60	15.60
1999 Floyd	29.84	97.56	0.35	3.03	88.06	30	10–15 Sept.	–5.30	24.50
1999 Gert	22.93	68.42	0.24	2.32	80.43	24	17–21 Sept.	–6.80	37.10
1999 Jose	3.93	112.99	1.61	3.6	9.52	10	22–24 Oct.	–1.70	5.10
2000 Alberto	5.39	98.43	0.7	3.77	10.32	4	9–11 Aug.	–3.10	13.50
2000 Florence	3.93	43.72	0.98	1.68	16.85	26	11–16 Sept.	–2.80	63.60
2000 Isaac	18.06	121.32	1	4.71	27.38	3	29 Sept.	–7.20	90.50
2000 Michael	3.93	28.96	0.65	1.13	24.89	7	17–18 Oct.	–6.50	79.70
2001 Erin	9.87	78.85	0.83	2.82	27.07	16	6–9 Sept.	–1.00	7.60
2001 Michelle	5.39	182.49	0.62	6.32	6.83	11	5–6 Nov.	–9.30	18.40

in the tropical waters off the African coast. Michael had the slowest transit speed of any storm examined, with Florence being the next slowest. Isaac had the second fastest transit speed. Florence and Isaac both had nondimensional storm speeds (S) near unity, indicating that inertial resonance may have contributed to the oceanic response.

[48] Given the observed relation between SST and chl-a responses (Figure 9), is the observed chl-a indicative only of entrainment of subsurface phytoplankton or of some combination of chl-a entrainment with a phytoplankton bloom resulting from entrained or upwelled nutrients? Because the DCM in summertime oligotrophic waters is generally shallower than the nutricline, it is possible that storm-induced mixing could entrain phytoplankton into surface waters without a concomitant injection of nutrients. However, the resulting post-storm surface chl-a response would dissipate

relatively quickly due to the lack of nutrients near the surface. Alternatively, if the storm-induced mixing entrained both phytoplankton and nutrients from below, then a more pronounced and persistent increase in surface chl-a would be observed because the entrained phytoplankton would benefit from both the entrained nutrients and the increased irradiance.

[49] As mentioned in section 2, the NODC chl-a profiles were annual means down to a depth of 100 m, so we could not test the alternate hypothesis that our observations were due only to entrainment of chl-a. However, we do note that the average time for the satellite-observed along-track area-averaged surface chl-a concentrations to fall from their hurricane-associated peaks to values closest to their pre-storm concentrations was about 3 weeks. The shortest chl-a restoration times were on the order of a few days and

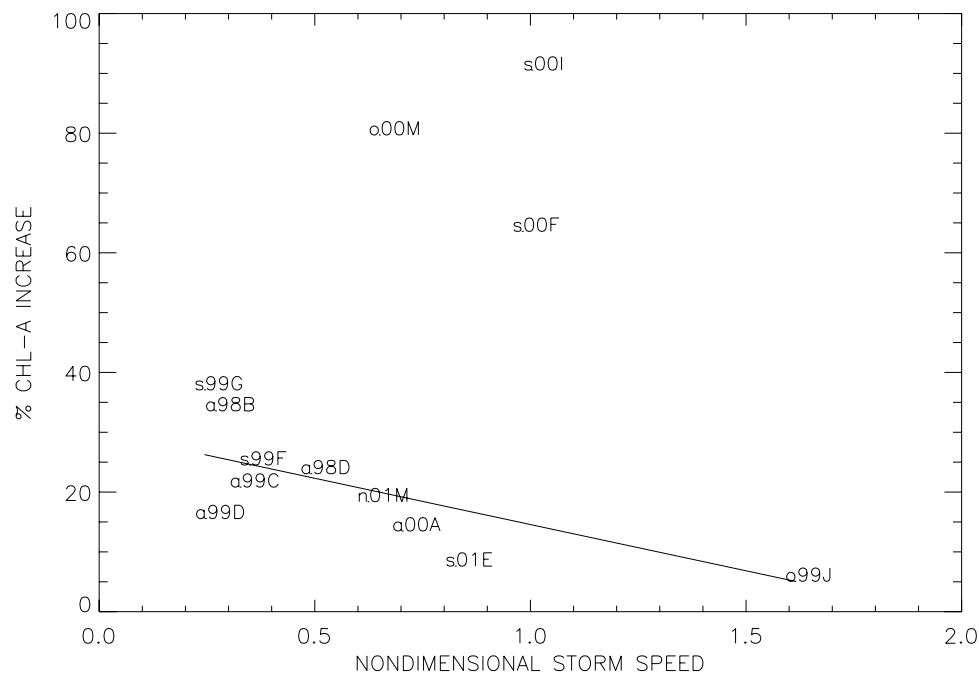


Figure 11. SeaWiFS-derived mean chlorophyll percent change and non-dimensional storm speed S for passage of each of the 13 storms through by 20°N , 78°W , 32°N , and 55°W . The labels indicate the first initial of the month the storm was within our box (lower case), the last two digits of the year, and the first initial of the storm name (upper case). The line is a linear least squares fit to all these points.

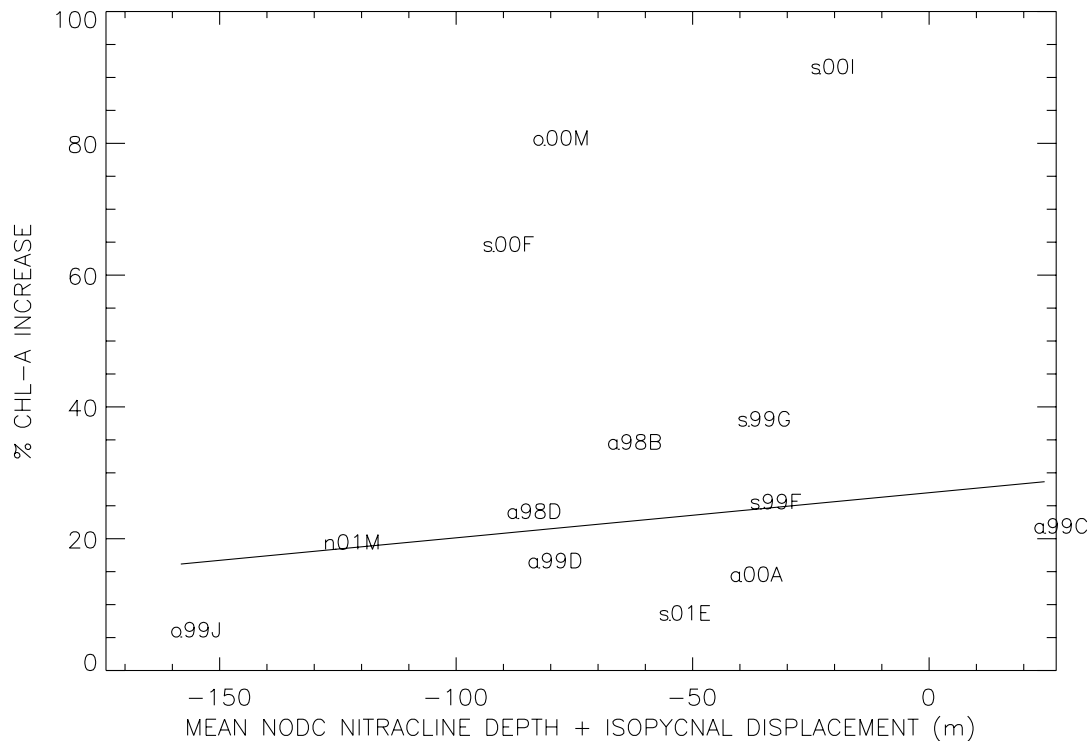


Figure 12. SeaWiFS-derived mean chlorophyll percent change is the ordinate and NODC-derived mean nitracline depth plus isopycnal displacement from the seasonal thermocline (η) is the abscissa. The line is a linear least squares fit to all these points. The labels indicate the first initial of the month the storm was within our box (lower case), the last two digits of the year, and the first initial of the storm name (upper case).

occurred with 2001 Michelle and 2000 Florence. Therefore it is possible that chl-a entrainment was dominant in these two cases, so that mixing dispersed the entrained chl-a without significant offset by a phytoplankton bloom producing chl-a that would have resulted in near-surface chl-a concentrations persisting for longer periods. The longer chl-a restoration times observed with the remaining 11 hurricanes are likely more consistent with at least the additional effect of a phytoplankton bloom induced by nutrient injection.

5. Conclusions

[50] A scientific understanding of the seasonal cycle of near-surface phytoplankton concentration and blooms has historically been constrained by fundamental in situ sampling limitations, which can result in significantly aliased characterizations of pelagic systems [Wiggert *et al.*, 1994]. In particular, ship-based sampling has been restricted to approximately monthly observations over the seasonal cycle [e.g., Steinberg *et al.*, 2001]. In situ sampling from ships has necessarily neglected characterizing the impact of strong wind events, especially hurricanes. As a consequence, contributions of hurricanes and mesoscale phenomena to the so-called mean state of oceanic ecosystems remains largely unresolved. Satellite observations are especially valuable in contributing to a reduction in this uncertainty.

[51] Recent observations by satellites, in addition to serendipitous hurricane passes over moorings, are providing growing evidence that episodic events, such as hurricanes

and eddies, play important roles in upper ocean ecology, including phytoplankton concentrations and species succession, biogeochemical cycling and global climate change [e.g., Marra *et al.*, 1990; Dickey *et al.*, 1993, 1998a, 1998b, 2001; McGillicuddy *et al.*, 1998; Bates *et al.*, 1998; McNeil *et al.*, 1999]. The recent availability of satellite-derived estimates of chl-a from SeaWiFS as well as AVHRR SST has provided an opportunity to explore the physical and biological responses to 13 hurricanes during the period 1998–2001. We used these estimates and focused our study on the western subtropical North Atlantic including the Sargasso Sea, whose oligotrophic waters are sensitive to mixing and entrainment processes yet remain uncomplicated by processes associated with proximity to coastal regions.

[52] The observed increases in chl-a in the wakes of these hurricanes ranged from a minimum of 5% to a maximum of 91%. This maximum is comparable to the spring bloom near Bermuda, which shows an increase of over 100% but with absolute magnitudes more pronounced than our observations of hurricane wakes [Banse and English, 1994]. The wake of increased chl-a coincides with the SST cooling distribution, forms within a few days of hurricane passage, and usually lasts for weeks following storm passage. Thus, for most of these hurricanes, the timing of the observed chl-a changes appears consistent with nutrient-induced phytoplankton blooms in addition to any chl-a entrainment that may also have occurred. This interpretation is also consistent with the results of a preliminary interdisciplinary modeling study [Babin *et al.*, 2002]. If verified,

the mechanism should be similar to that for blooms observed in situ with, for example, coastal upwelling events.

[53] Of the 13 hurricanes examined, three (Florence, Isaac, and Michael) appeared to be outliers in that their post-storm chl-a increases relative to their SST decreases were much larger than for the other storms. One common feature of these three storms was their relatively small hurricane-force wind radii. Two of them had the weakest mean wind speed and the smallest hurricane-force wind radii of all the storms examined. Florence had a short post-storm surface chl-a restoration time (a week), but the other two hurricanes had restoration times of about 2 weeks or more. One possible explanation may be that these three storms contained significant quantities of entrained dust and that the resulting wet deposition of iron enhanced the effects of these storms. Hurricanes have been shown to entrain Saharan dust (e.g., see http://visibleearth.nasa.gov/Atmosphere/Aerosols/Dust_Ash_15.html), and a computer model image on that same web page shows that Saharan dust can extend as far north as Spain. While Isaac formed as a tropical system close to Africa (11.7°N, 23.7°W), Florence (30.4°N, 72.4°W) and Michael (29.8°N, 70.9°W) both formed from non-tropical lows south of Bermuda. Of the 13 storms examined, Cindy formed the closest to Africa (13.6°N, 19.4°W).

[54] Perhaps a more likely explanation of our three outliers involves the fact that Florence and Isaac had nondimensional storm speeds very close to unity so that the chl-a responses were more affected by inertial resonance and the fact that Michael was the slowest moving of all 13 storms studied. In addition, Florence and Michael formed the farthest north and developed from subtropical depressions associated with cold frontal passages. Prior to the development of these two hurricanes, the passages of cold fronts over the northern Sargasso Sea in the future storm paths occurred. It is likely that the elevated air-sea temperature gradient associated with these atmospheric fronts led to increased heat flux that stimulated convective mixing that, in turn, initiated the erosion of water column stratification. Such a breakdown in stratification would allow for greater nutrient entrainment during the subsequent hurricane passage and the more pronounced phytoplankton response observed in the SeaWiFS imagery. Unfortunately, we do not have enough information to provide an entirely consistent and verified picture of what differences in these three storms led to their larger post-storm chl-a increases.

[55] Simple models of the biology of the mixed layer relate chl-a concentration to the strength and persistence of the surface winds. Indeed, we find that several physical parameters related to storm intensity, including wind strength and storm radius, are positively correlated with post-storm, satellite-derived chl-a increases. However, the results indicate a complex relationship between physical processes of mixing and entrainment and the intensity of the biological response. This is consistent with a past interdisciplinary modeling study that demonstrated a nonlinear enhancement of nutrient entrainment associated with elevated, time-varying surface winds [Klein and Coste, 1984]. The application of interdisciplinary models that include a more complex ecosystem component would significantly advance our understanding of phytoplankton response to hurricane passage.

[56] Although a chl-a increase has often been observed in other upwelling areas, we believe that this is the first documented satellite observation of this phenomenon in association with the cool wakes of hurricanes in the deep ocean. While the Sargasso Sea may be considered an ocean desert due to its low levels of nutrients, new production is maintained at levels of $50 \text{ g C m}^{-2} \text{ yr}^{-1}$ [e.g., McGillicuddy *et al.*, 1998]. It is possible that the three to four hurricanes that cross this region on average each year may contribute to the region's annual new production budget at a level similar to the estimated mesoscale eddy contribution [McGillicuddy and Robinson, 1997]. Because climate changes associated with El Niño Southern Oscillation [Gray, 1984] and global warming [Emanuel, 1987; Saunders and Harris, 1997] may influence the frequency and intensity of these storms, there may be important contributions to climate resulting from storm-induced biological and biogeochemical activity in the oligotrophic subtropical oceans [e.g., Bates *et al.*, 1998]. Development of coupled climate models will likely be necessary to address this issue. Because of the lack of interdisciplinary subsurface data sets, we cannot state conclusively that our observed changes in chl-a are the result of hurricane-induced nutrient injections and/or other effects such as entrainment or upwelling of waters with high chl-a concentrations. However, our results can serve to stimulate and guide future multiplatform field, satellite, and modeling studies that would advance our understanding of hurricane and typhoon influence on upper ocean ecosystems and biogeochemistry.

Appendix A: Satellite Data Used in This Study

[57] SeaWiFS was designed to study ocean pigments, especially those associated with phytoplankton. It uses an eight-band spectroradiometer with a nominal spatial resolution of 1 km at nadir and a revisit time of 1 day. The level-three data products are binned to a 9×9 km spatial grid and include chl-a concentration, which is commonly considered a direct proxy for the magnitude of the surface ocean's phytoplankton population. The NASA Goddard Space Flight Center SeaWiFS Project Office derives chl-a from water-leaving radiances after atmospheric correction using empirical algorithms [O'Reilly *et al.*, 1998]. The level-three chl-a values we obtained from NASA were derived from an algorithm (called OC4 by O'Reilly *et al.* [1998]) that uses a maximum band ratio technique and that has been validated for the open ocean by comparison with in situ data. When this algorithm was parameterized with over 2800 data sets of coincident in situ chl-a measurements, the correlation between them was 0.9 with a slope of unity and zero intercept over a wide range of chl-a values [O'Reilly *et al.*, 2000]. While the average percent error over all the data for both coastal and open ocean waters was around 24%, the scatter about this line was much less at chl-a values below about 0.5 mg m^{-3} , the regime in which our measurements were made. SeaWiFS data have proven very useful in assessing changes in chl-a concentrations, such as those caused by hurricane-induced runoff in Puerto Rico [Gilbes *et al.*, 2001]. While other ocean color imaging satellites are now in orbit, cross-calibration has not yet been completed. Therefore, for the sake of consistency and for the 1998–2001 years of interest, we have chosen to use only SeaWiFS

data for this study. To minimize the effects of clouds, the SeaWiFS data products use the 865-nm channel for cloud detection. Because the Sargasso Sea SSTs during our study were greater than 20°C and high level clouds are much cooler, these data should have minimal cloud contamination. In order to use near-real time data while further minimizing the effects of any cloud-contaminated pixels, the level-three 8-day mean chl-a SeaWiFS products were used in this study.

[58] The Johns Hopkins University Applied Physics Laboratory (JHU/APL) received AVHRR data broadcast from the NOAA-12 and NOAA-14 satellites during the years 1998–2001. The AVHRR instrument has five channels and a maximum resolution of 1 km near nadir. JHU/APL uses TeraScan (SeaSpace Corporation, San Diego, California) software to register the satellite data to geographic coordinates and to derive SST images using an algorithm described by Bernstein [1982]. Details of this image processing are described by Monaldo *et al.* [1997]. Because it is typical for clouds to change hourly and SST features to change on the order of several days, we generate composite SST images by combining the maximum SST per pixel from both NOAA satellites over a period of 7 days. Because clouds are colder than the SSTs in the Sargasso Sea during summer and autumn, this compositing removes most of the cloud-contaminated pixels. Therefore the SSTs are not 7-day means but are believed to be sufficiently representative of the SST during each 7-day period. It should be noted that, during the times of hurricane passage through the box, the sea surface beneath the storm is obscured by clouds so that, depending on the forward speed of the hurricane, the 8-day chl-a means (obtained from NASA) along the track may really be means of less than 8 days and the 7-day SST composite values (obtained from JHU/APL) along the track may really be less than 7 days.

[59] **Acknowledgments.** The authors would like to express their sincere appreciation to Ray Sterner of JHU/APL for development of many of the image processing computer programs used in this work. The authors also would like to thank the SeaWiFS Project (Code 970.2) and the Distributed Active Archive Center (Code 902) at the NASA Goddard Space Flight Center, Greenbelt, Maryland, for the production and distribution of the ocean color data, respectively. Use of these data is in accord with the SeaWiFS Research Data Use Terms and Conditions Agreement. This work was supported in part by NASA grant NASA960912 to J. C. and by a JHU/APL Stuart Janney Fellowship to S. B.. Support of T. D.'s research has been provided by the U.S. Office of Naval Research, National Science Foundation, NASA, the National Ocean Partnership Program, and the University of California, Santa Barbara.

References

- Anthes, R. A., and S. W. Chang (1978), Response of the hurricane boundary layer to changes in sea surface temperature in a numerical model, *J. Atmos. Sci.*, **35**, 1240–1255.
- Babin, S. M., J. A. Carton, T. D. Dickey, and J. D. Wiggert (2002), Hurricane-induced phytoplankton blooms in the Sargasso Sea, paper presented at the 2002 AGU/ASLO Ocean Sciences Meeting, AGU, Honolulu, Hawaii.
- Banase, K., and D. C. English (1994), Seasonality of coastal zone color scanner phytoplankton pigment in the offshore oceans, *J. Geophys. Res.*, **99**, 7323–7345.
- Bates, N. R., A. H. Knap, and A. F. Michaels (1998), Contribution of hurricanes to local and global estimates of air-sea exchange of CO₂, *Nature*, **395**, 58–61.
- Bernstein, R. L. (1982), Sea surface temperature estimation using the NOAA-6 advanced very high resolution radiometer, *J. Geophys. Res.*, **87**, 9455–9465.
- Black, P. G., and G. J. Holland (1995), The boundary layer of tropical cyclone Kerry (1979), *Mon. Weather Rev.*, **123**, 2007–2028.
- Brand, S. (1971), The effects on a tropical cyclone of cooler surface waters due to upwelling and mixing produced by a prior tropical cyclone, *J. Appl. Meteorol.*, **10**, 865–874.
- Conkright, M. E., T. D. O'Brien, S. Levitus, T. P. Boyer, C. Stephens, and J. I. Antonov (1998), *World Ocean Atlas 1998*, vol. 10, *Nutrient and Chlorophyll of the Atlantic Ocean*, NOAA Atlas NESDIS 36, Natl. Oceanic and Atmos. Admin., Silver Spring, Md. (Available at http://www.nodc.noaa.gov/OC5/WOA98F/woaf_cd/doc/readme.html)
- Conte, M. H., T. D. Dickey, J. C. Weber, R. J. Johnson, and A. H. Knap (2003), Transient physical forcing of pulsed export of bioactive material to the deep Sargasso Sea, *Deep Sea Res., Part I*, **50**, 1157–1187.
- Dickey, T. D., and P. Falkowski (2002), Solar energy and its biological-physical interactions in the sea, in *The Sea*, vol. 12, *Biological-Physical Interactions in the Sea*, edited by A. R. Robinson, J. J. McCarthy, and B. J. Rothschild, chap. 9, 401–440, John Wiley, Hoboken, N. J.
- Dickey, T. D., and J. J. Simpson (1983), The sensitivity of upper ocean structure to time varying wind direction, *Geophys. Res. Lett.*, **10**, 133–136.
- Dickey, T. D., et al. (1993), Seasonal variability of bio-optical and physical properties in the Sargasso Sea, *J. Geophys. Res.*, **98**, 865–898.
- Dickey, T. D., et al. (1998a), Initial results from the Bermuda Testbed Mooring Program, *Deep Sea Res., Part I*, **45**, 771–794.
- Dickey, T. D., D. Frye, J. McNeil, D. Manov, N. Nelson, D. Sigurdson, H. Jannasch, D. Siegel, A. F. Michaels, and R. J. Johnson (1998b), Upper-ocean temperature response to Hurricane Felix as measured by the Bermuda Testbed Mooring, *Mon. Weather Rev.*, **126**, 1195–1201.
- Dickey, T. D., et al. (2001), Physical and biogeochemical variability from hours to years at the Bermuda Testbed Mooring site: June 1994–March 1999, *Deep Sea Res., Part II*, **48**, 2105–2131.
- Elsner, J. B. (2003), Tracking hurricanes, *Bull. Am. Meteorol. Soc.*, **84**(3), 353–356.
- Emanuel, K. A. (1987), The dependence of hurricane intensity on climate, *Nature*, **326**, 483–485.
- Gilbes, F., R. A. Armstrong, R. M. T. Webb, and F. E. Müller-Karger (2001), SeaWiFS helps assess hurricane impact on phytoplankton in Caribbean Sea, *Eos Trans. AGU*, **82**, 529, 533.
- Gray, W. M. (1984), Atlantic seasonal hurricane frequency: I. El Niño and 30 mb quasi-biennial oscillation influences, *Mon. Weather Rev.*, **112**, 1649–1668.
- Greatbatch, R. J. (1984), On the response of the ocean to a moving storm: Parameters and scales, *J. Phys. Oceanogr.*, **14**, 59–78.
- Hazelworth, J. B. (1968), Water temperature variations resulting from hurricanes, *J. Geophys. Res.*, **73**, 5105–5123.
- Klein, P., and B. Coste (1984), Effects of wind-stress variability on nutrient transport into the mixed layer, *Deep Sea Res., Part A*, **31**, 21–37.
- Marra, J., R. R. Bidigare, and T. D. Dickey (1990), Nutrients and mixing, chlorophyll, and phytoplankton growth, *Deep Sea Res.*, **37**, 127–143.
- McClain, C. (2001), *Encyclopedia of Ocean Sciences*, vol. 4, *Ocean Color From Satellites*, edited by J. H. Steele, K. K. Turekian, and S. A. Thorpe, pp. 1946–1959, Academic, San Diego.
- McGillicuddy, D. J., and A. R. Robinson (1997), Eddy-induced nutrient supply and new production in the Sargasso Sea, *Deep Sea Res., Part I*, **44**, 1427–1450.
- McGillicuddy, D. J., A. R. Robinson, D. A. Siegel, H. W. Jannasch, R. Johnson, T. D. Dickey, J. McNeil, A. F. Michaels, and A. H. Knap (1998), Influence of mesoscale eddies on new production in the Sargasso Sea, *Nature*, **394**, 263–266.
- McGillicuddy, D. J., V. K. Kosnyrev, J. P. Ryan, and J. A. Yoder (2001), Covariation of mesoscale ocean color and sea-surface temperature patterns in the Sargasso Sea, *Deep Sea Res., Part II*, **48**, 1823–1836.
- McNeil, J. D., H. W. Jannasch, T. D. Dickey, D. McGillicuddy, M. Brzezinski, and C. M. Sakamoto (1999), New chemical, bio-optical and physical observations of upper ocean response to the passage of a mesoscale eddy off Bermuda, *J. Geophys. Res.*, **104**, 15,537–15,548.
- Monaldo, F. M., T. D. Sikora, S. M. Babin, and R. E. Sterner (1997), Satellite imagery of sea surface temperature cooling in the wake of Hurricane Edouard, *Mon. Weather Rev.*, **125**, 2716–2721.
- Morel, A., and L. Prieur (1977), Analysis of variations in ocean color, *Limnol. Oceanogr.*, **22**, 709–722.
- O'Reilly, J. E., S. Maritorena, B. G. Mitchell, D. A. Siegel, K. L. Carder, S. A. Garver, M. Kahru, and C. McClain (1998), Ocean color chlorophyll algorithms for SeaWiFS, *J. Geophys. Res.*, **103**, 24,937–24,953.
- O'Reilly, J. E., et al. (2000), SeaWiFS postlaunch calibration and validation analyses, *SeaWiFS Postlaunch Tech. Rep. Ser.*, vol. 11, part 3, edited by S. Hooker and E. Firestone, *NASA/TM-2000-206892*, 49 pp., NASA Goddard Space Flight Cent., Greenbelt, Md.
- Price, J. F. (1981), Upper ocean response to a hurricane, *J. Phys. Oceanogr.*, **11**, 153–175.
- Price, J. F., T. B. Sanford, and G. Z. Forristall (1994), Forced stage response to a moving hurricane, *J. Phys. Oceanogr.*, **24**, 233–260.

- Sanford, T. B., P. G. Black, J. R. Haustein, J. W. Feeney, G. Z. Forristall, and J. F. Price (1987), Ocean response to a hurricane: I. Observations, *J. Phys. Oceanogr.*, *17*, 2065–2083.
- Saunders, M. A., and A. R. Harris (1997), Statistical evidence links exceptional 1995 Atlantic hurricane season to record sea warming, *Geophys. Res. Lett.*, *24*, 1255–1258.
- Shay, L. K., and R. L. Elsberry (1987), Near-inertial ocean current response to Hurricane Frederick, *J. Phys. Oceanogr.*, *17*, 1249–1269.
- Shay, L. K., R. L. Elsberry, and P. G. Black (1989), Vertical structure of the ocean current response to a hurricane, *J. Phys. Oceanogr.*, *19*, 649–669.
- Shay, L. K., S. W. Chang, and R. L. Elsberry (1990), Free surface effects on the near-inertial ocean current response to a hurricane, *J. Phys. Oceanogr.*, *20*, 1405–1424.
- Siegel, D. A., R. Iturriaga, R. R. Bidigare, R. C. Smith, H. Pak, T. D. Dickey, J. Marra, and K. S. Baker (1990), Meridional variations of the springtime phytoplankton community in the Sargasso Sea, *J. Mar. Res.*, *48*, 379–412.
- Siegel, D. A., S. C. Doney, and J. A. Yoder (2002), The North Atlantic spring phytoplankton bloom and Sverdrup's critical depth hypothesis, *Science*, *296*, 730–732.
- Sousa, F. M., and A. Bricaud (1992), Satellite-derived phytoplankton pigment structures in the Portuguese upwelling area, *J. Geophys. Res.*, *97*, 11,343–11,356.
- Steinberg, D. K., C. A. Carlson, N. R. Bates, R. J. Johnson, A. F. Michaels, and A. H. Knap (2001), Overview of the US JGOFS Bermuda Atlantic Time-series Study (BATS): A decade-scale look at ocean biology and biogeochemistry, *Deep Sea Res., Part II*, *48*, 1405–1447.
- Stramma, L., P. Cornillon, and J. F. Price (1986), Satellite observations of sea surface cooling by hurricanes, *J. Geophys. Res.*, *91*, 5031–5035.
- Strass, V. H. (1992), Chlorophyll patchiness caused by mesoscale upwelling at fronts, *Deep Sea Res.*, *39*, 75–96.
- Talley, L. D., and M. E. Raymer (1982), Eighteen degree water variability, *J. Mar. Res.*, *40*, 757–775.
- Varela, R. A., A. Cruzado, J. Tintore, and E. G. Ladona (1992), Modeling the deep-chlorophyll maximum: A coupled physical-biological approach, *J. Mar. Res.*, *50*, 441–463.
- Wiggert, J., T. D. Dickey, and T. Granata (1994), The effect of temporal undersampling on primary production estimates, *J. Geophys. Res.*, *99*, 3361–3371.
- Zedler, S. E., T. D. Dickey, S. C. Doney, J. F. Price, X. Yu, and G. L. Mellor (2002), Analyses and simulations of the upper ocean's response to Hurricane Felix at the Bermuda Testbed Mooring site: August 13–23, 1995, *J. Geophys. Res.*, *107*, 3232, doi:10.1029/2001JC000969.
-
- S. M. Babin, Johns Hopkins University Applied Physics Laboratory, Laurel, MD 20723-6099, USA. (steven.babin@jhuapl.edu)
- J. A. Carton, Department of Meteorology, University of Maryland, College Park, MD 20742, USA. (carton@atmos.umd.edu)
- T. D. Dickey, Ocean Physics Laboratory, University of California, Santa Barbara, 6487 Calle Real, Suite A, Goleta, CA 93117, USA. (tommy.dickey@opl.ucsb.edu)
- J. D. Wiggert, Center for Coastal Physical Oceanography, Old Dominion University, Norfolk, VA 23539, USA. (jwiggert@ccpo.odu.edu)